Supplementary Information

Mechanism of Water Oxidation by Non-Heme Iron Catalysts when Driven with Sodium Periodate

Alexander Rene Parent,[a*] *Takashi Nakazono,*[b] *Shu Lin,*[b] *Satoshi Utsunomiya*[b] *and Ken Sakai*[a,b,c*]

[a] International Institute for Carbon-Neutral Energy Research (WPI-I2CNER), Kyushu University, Motooka 744, Nishi-ku, Fukuoka 819-0395, Japan

[b] Department of Chemistry, Faculty of Sciences, Kyushu University, 6-10-1 Hakozaki, Higashi-ku, Fukuoka 812-8581, Japan

[c] Center for Molecular Systems (CMS), Kyushu University, Motooka 744, Nishi-ku, Fukuoka 819-0395, Japan

E-mail: aparent@chem.kyushu-univ.jp; ksakai@chem.kyushu-univ.jp

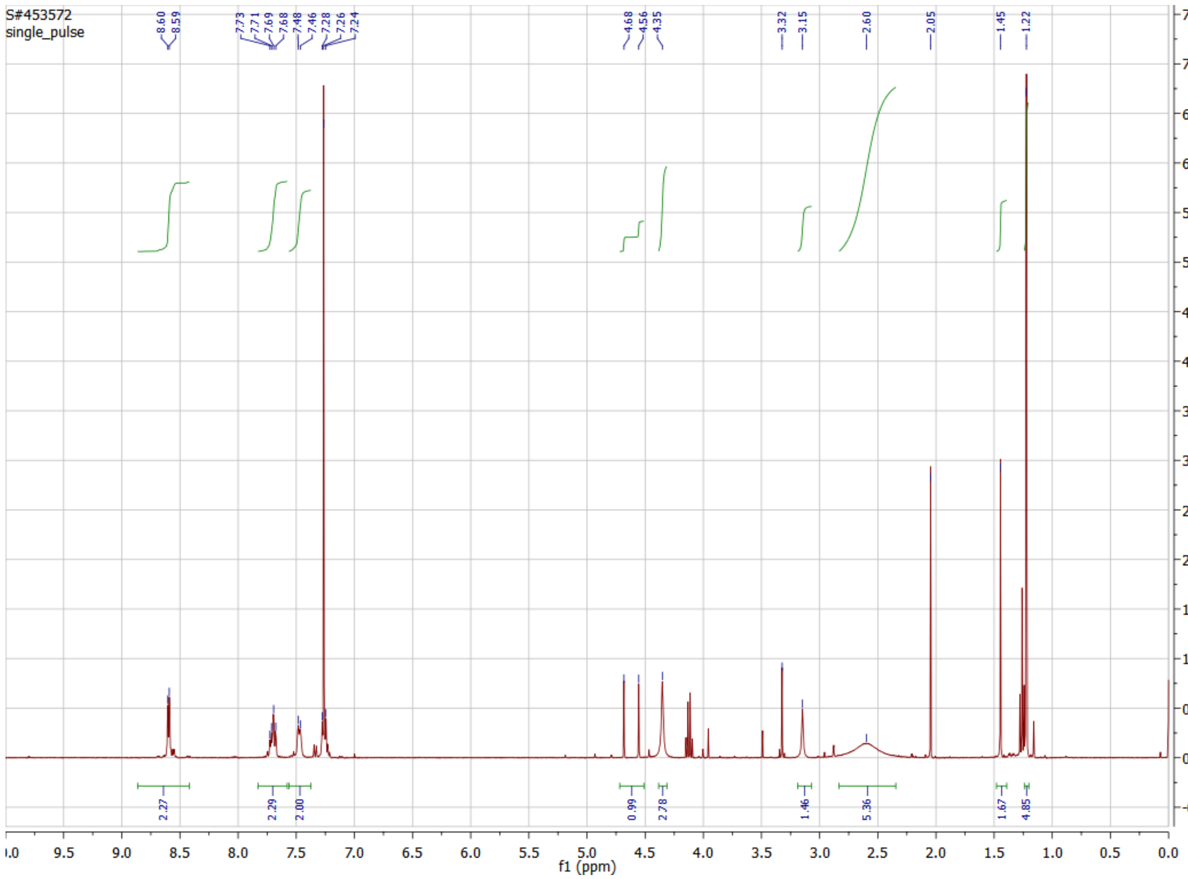

Figure S1. NMR Spectra of the BPyA ligand in $CDCl_3$.

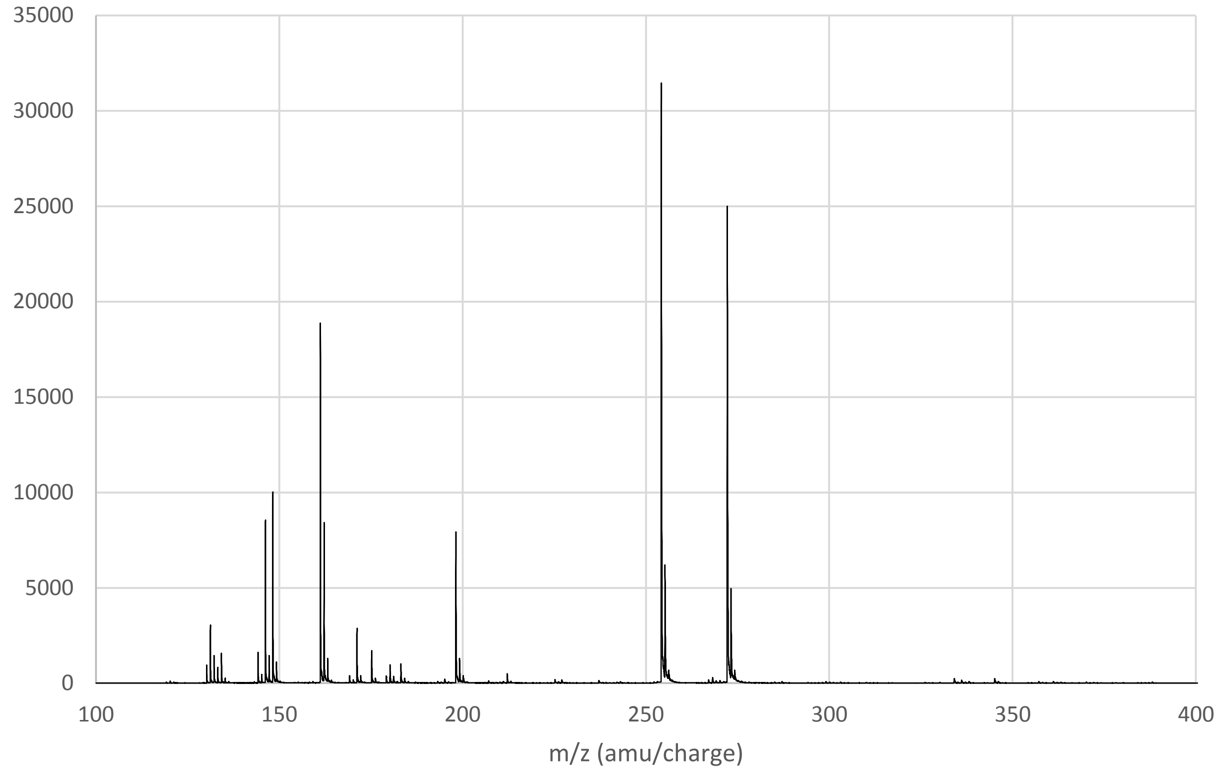

Figure S2. ESI-MS of BPyA in MeOH, the peak at 272 m/z corresponds to LH^+.

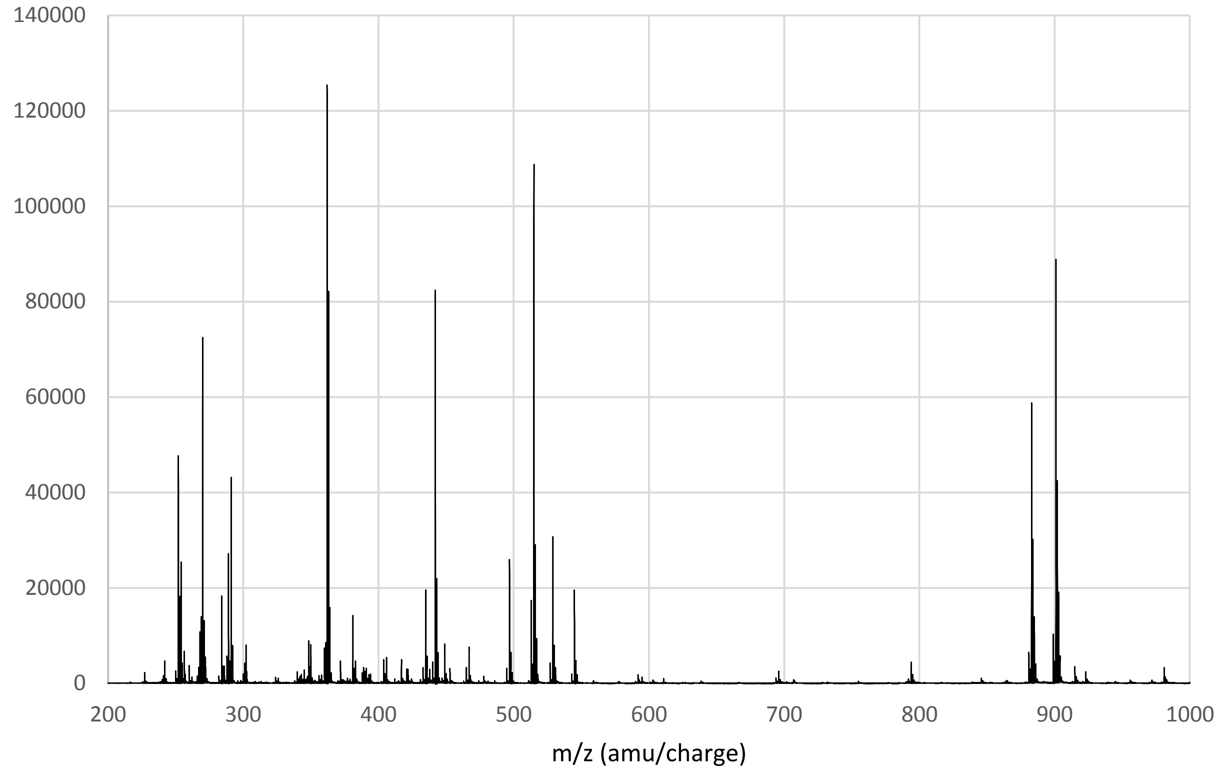

Figure S3. ESI-MS of **1** in MeOH. The peak at 901 m/z corresponds to μ-(SO_4)-μ-(O)-[Fe(TPA)]$_2$(HSO_4)$^+$. The peak at 883 m/z corresponds to μ-(SO_4)[Fe(TPA)]$_2$(SO_4)$^+$. The peak at m/z 515 corresponds to μ-(O)-(TPA)Fe_2(HSO_4)$^+$. The peak at m/z 442 corresponds to Fe(TPA)$(OH)_2$$(MeOH)_2$$^+$. The peak at m/z 291 corresponds to $TPAH^+$.

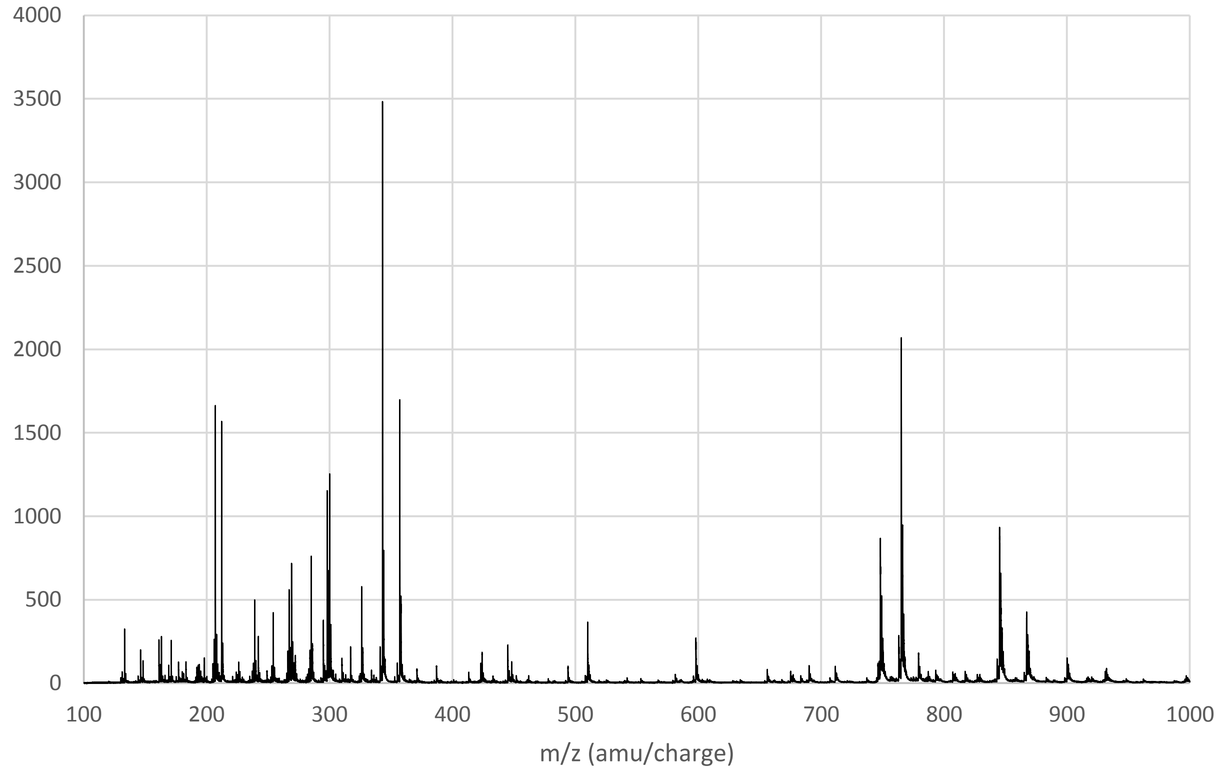

Figure S4. ESI-MS of **2** in methanol. The peak at 765.2 m/z corresponds to a sulfate or hydroxide bridged Fe dimer of the formula $(OH)(SO_4)[Fe(BPyA)]_2^+$. The peak at 748.1 m/z corresponds to a sulfate bridged Fe dimer of the formula μ-$(SO_4)[Fe(BPyA)]_2^+$. The peak at 854.1 m/z corresponds to a sulfate bridged Fe dimer of the formula μ-$(SO_4)(HSO_4)[Fe(BPyA)]_2^+$. The peak at 357.1 m/z corresponds to $Fe(BPyA)(OMe)^+$. The major peak at 343.1 m/z corresponds to $Fe(BPyA)(OH)^+$.

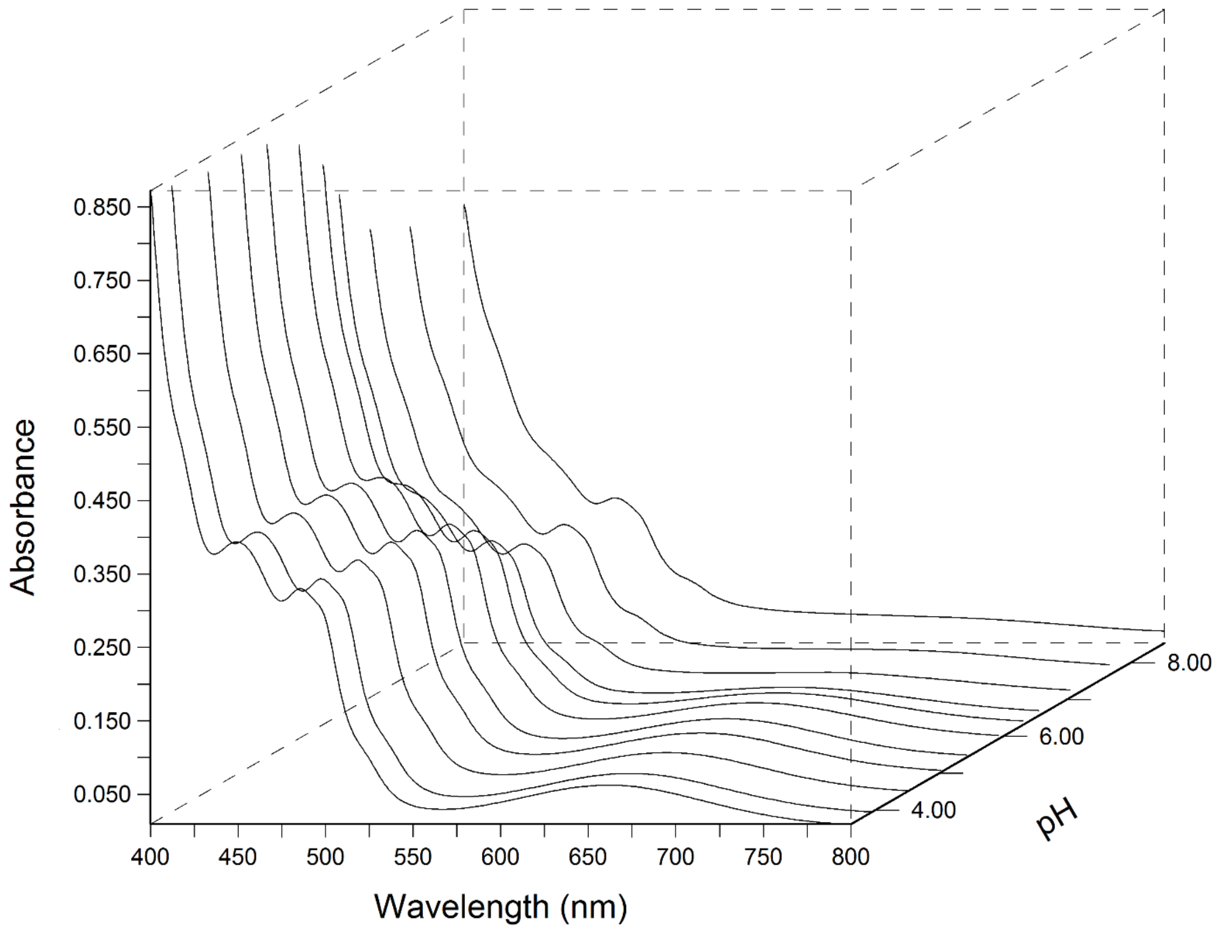

Figure S5. Visible spectra during pH titration of 10 mL 523 µM **1** with 10 mM NaOH.

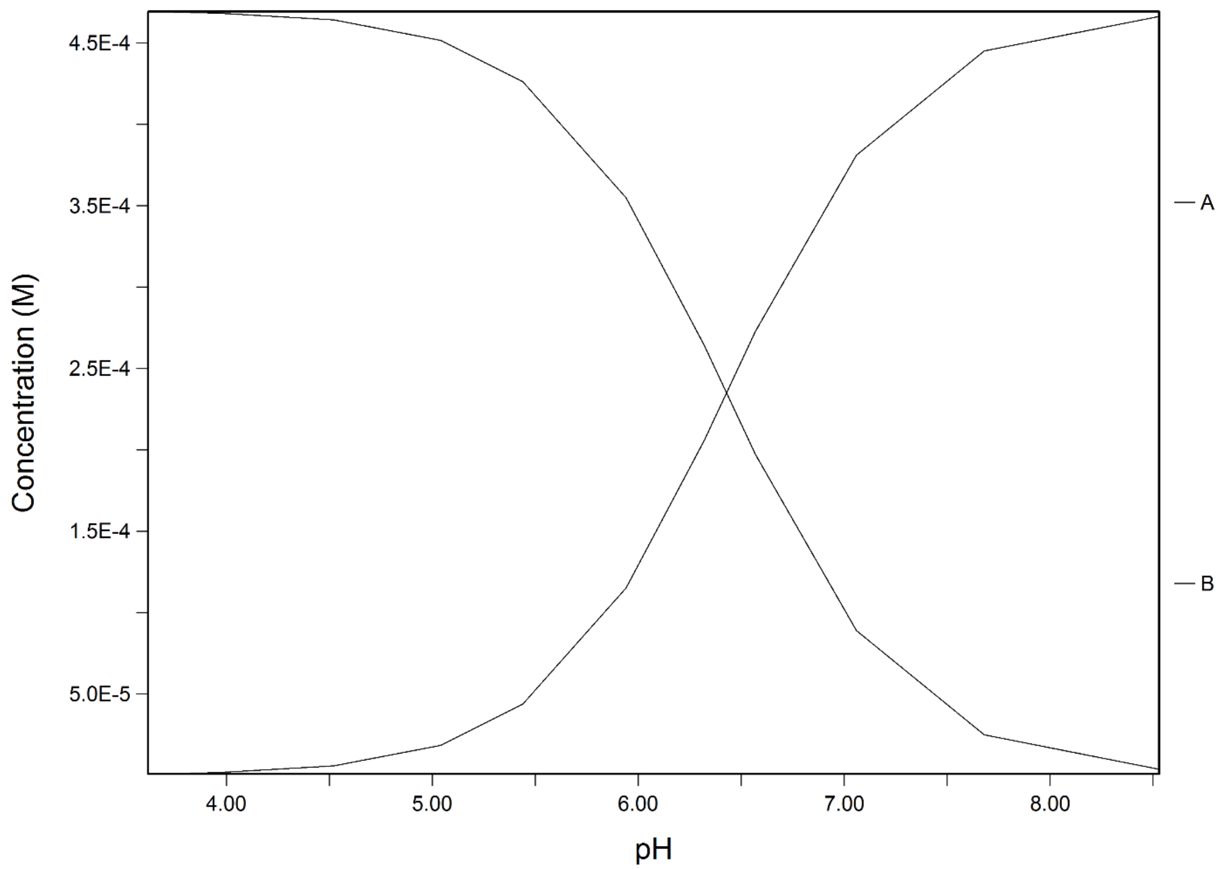

Figure S6. Species concentrations predicted by the SPECFIT fitting of the pH titration of 10 mL 523 μM **1** with 10 mM NaOH.

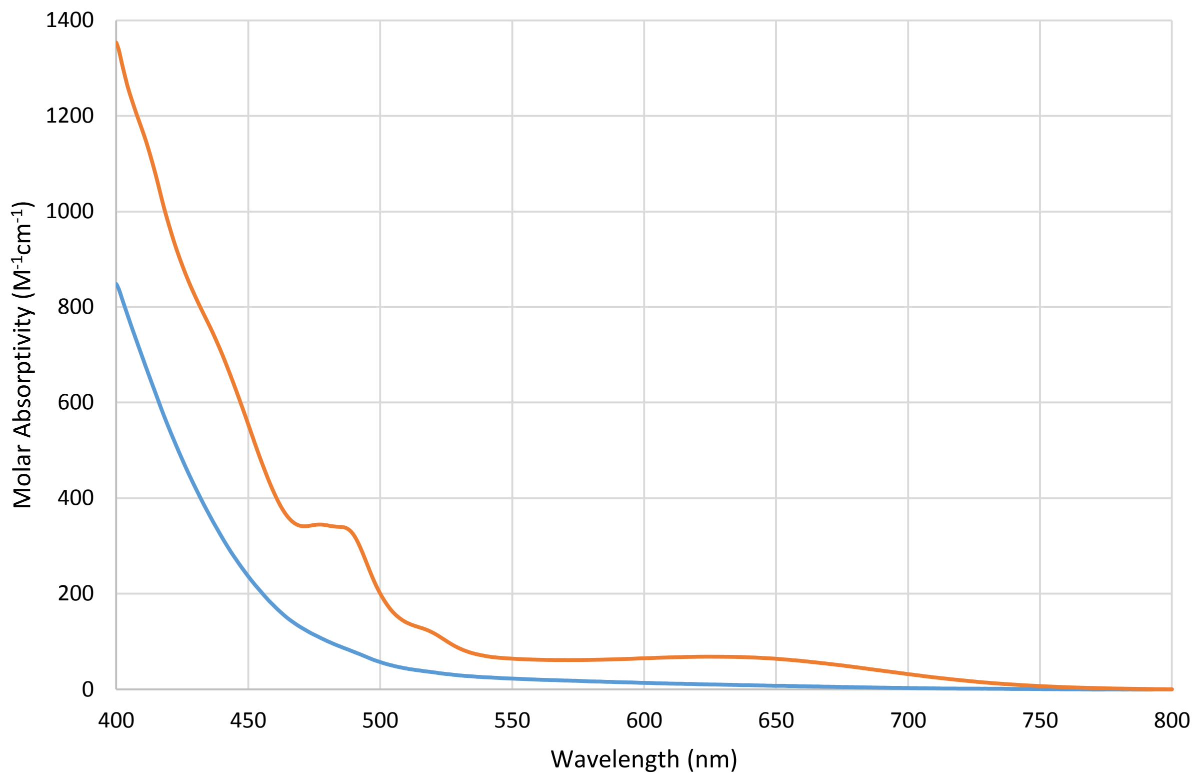

Figure S7. Calculated visible spectra of monomeric (blue) and dimeric (orange) **2** by the SPECFIT global fitting of the concentration dependent visible absorption of **2** (Fig. 3b).

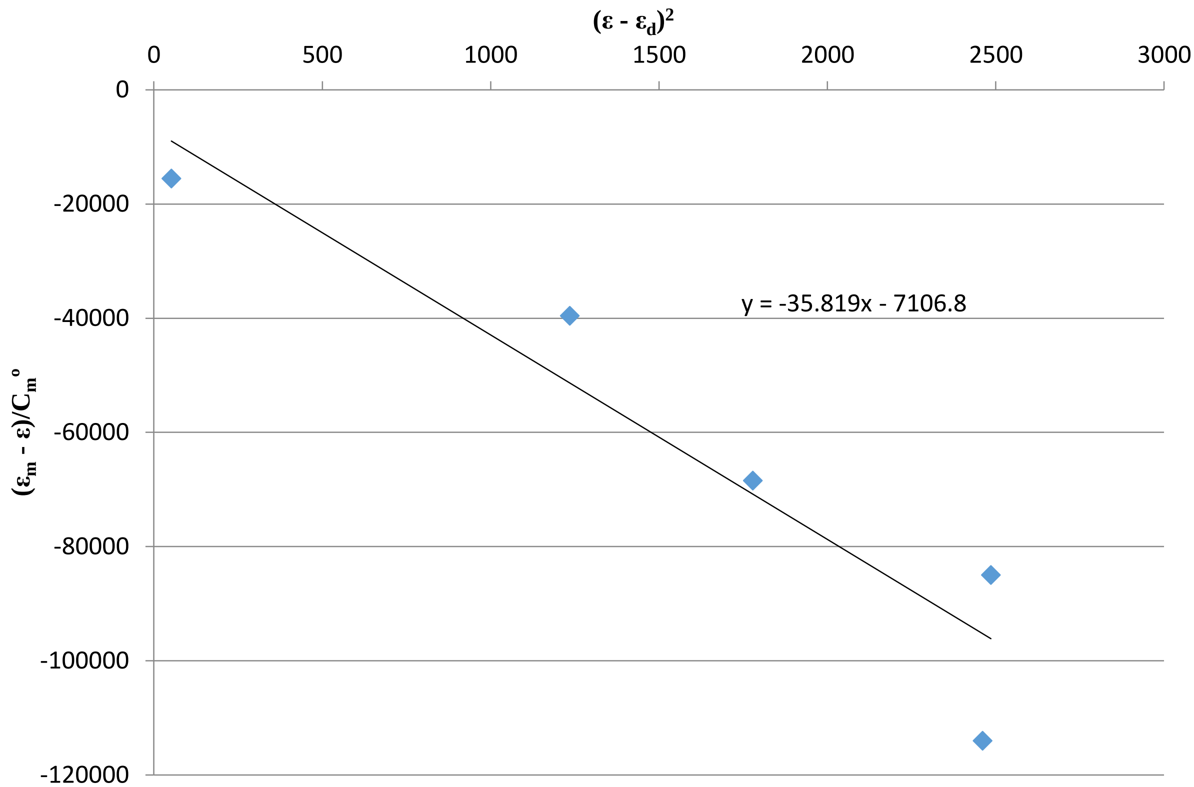

Figure S8. Linear fit to $(\varepsilon_m - \varepsilon)/C_m°$ vs. $(\varepsilon - \varepsilon_d)^2$ at 518 nm for **2**.

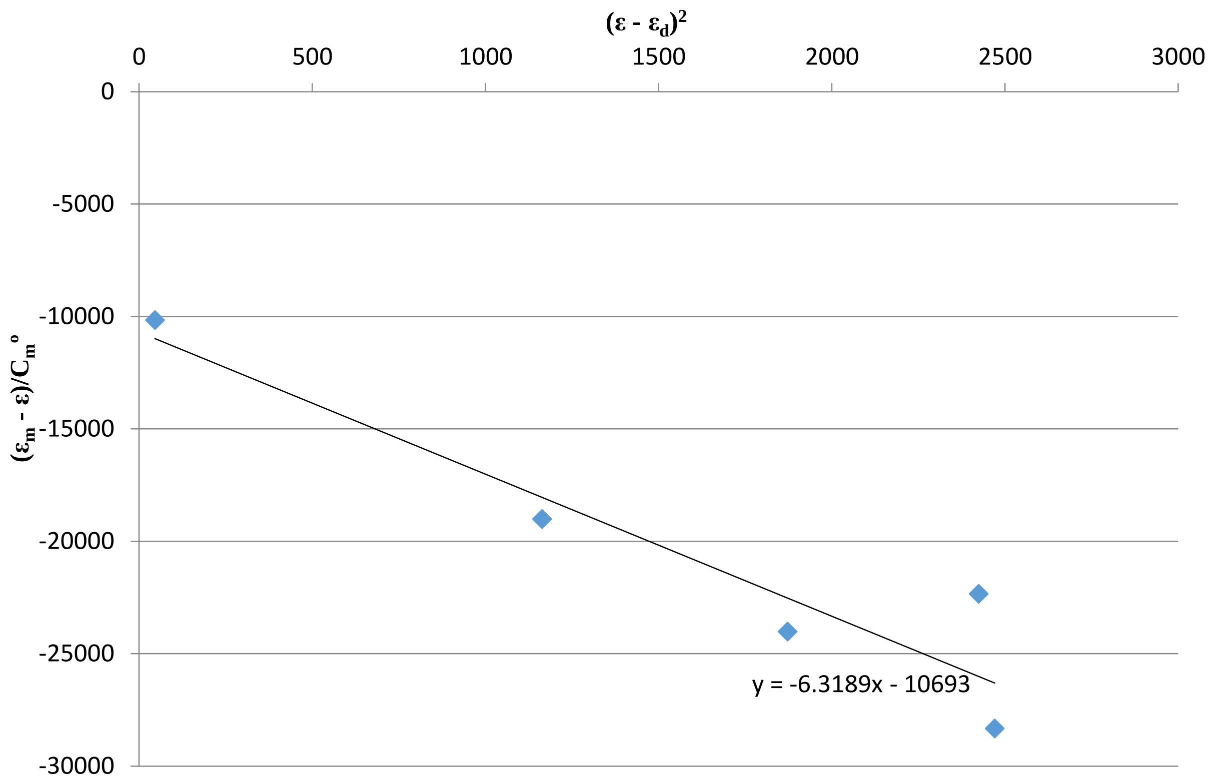

Figure S9. Linear fit to $(\varepsilon_m - \varepsilon)/C_m^\circ$ vs. $(\varepsilon - \varepsilon_d)^2$ at 632 nm for **2**.

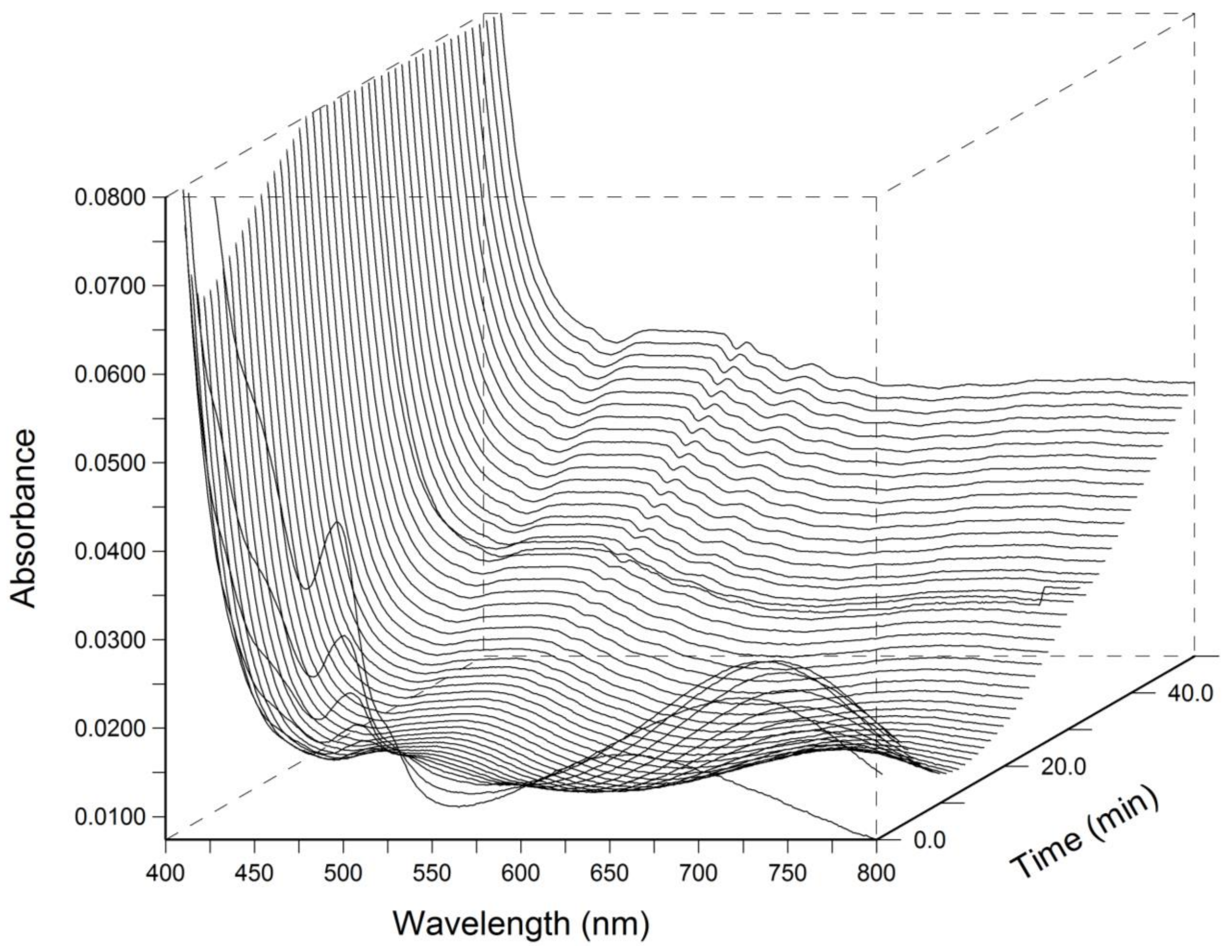

Figure S10. Visible time-course upon addition of 94 µM **1** to 10.0 mM $NaIO_4$.

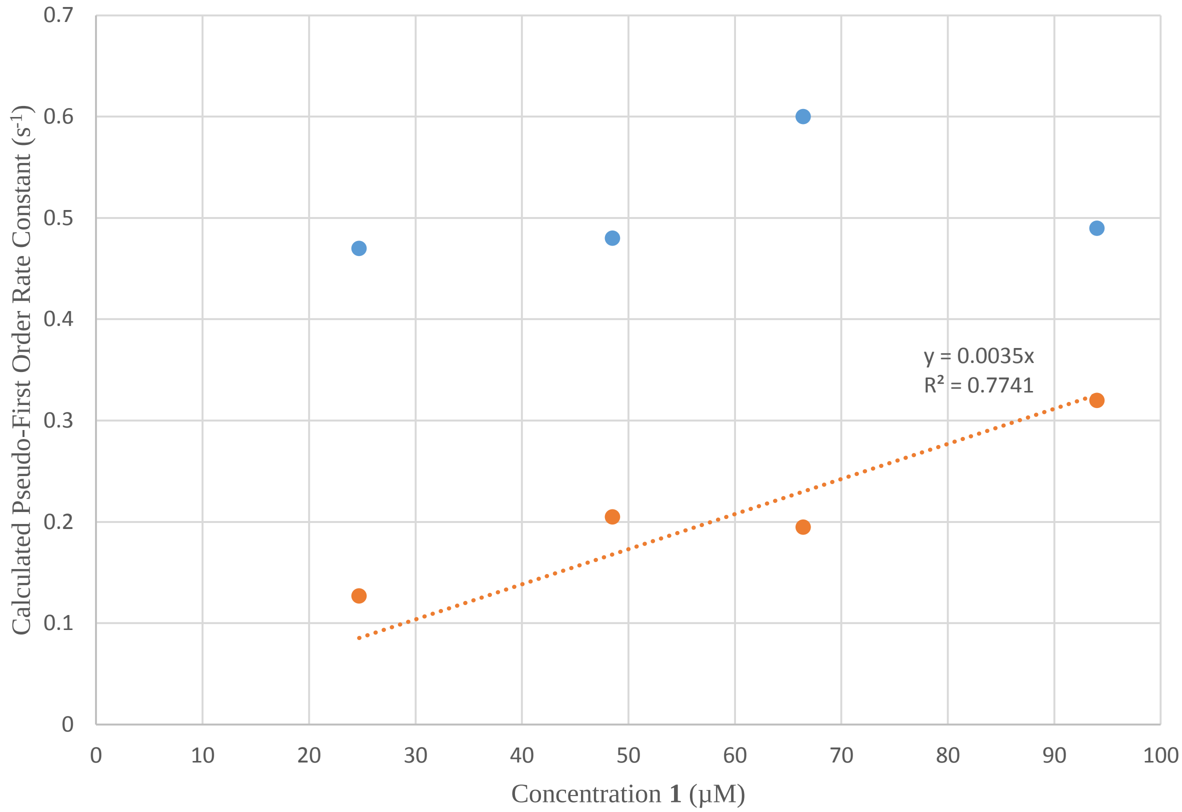

Figure S11. Calculated rate constants vs. concentration of **1** for k_1 (blue), and K_2 (orange) in 10.0 mM $NaIO_4$, pH 5.0. Dotted line shows linear fit to k_2 vs. [**1**].

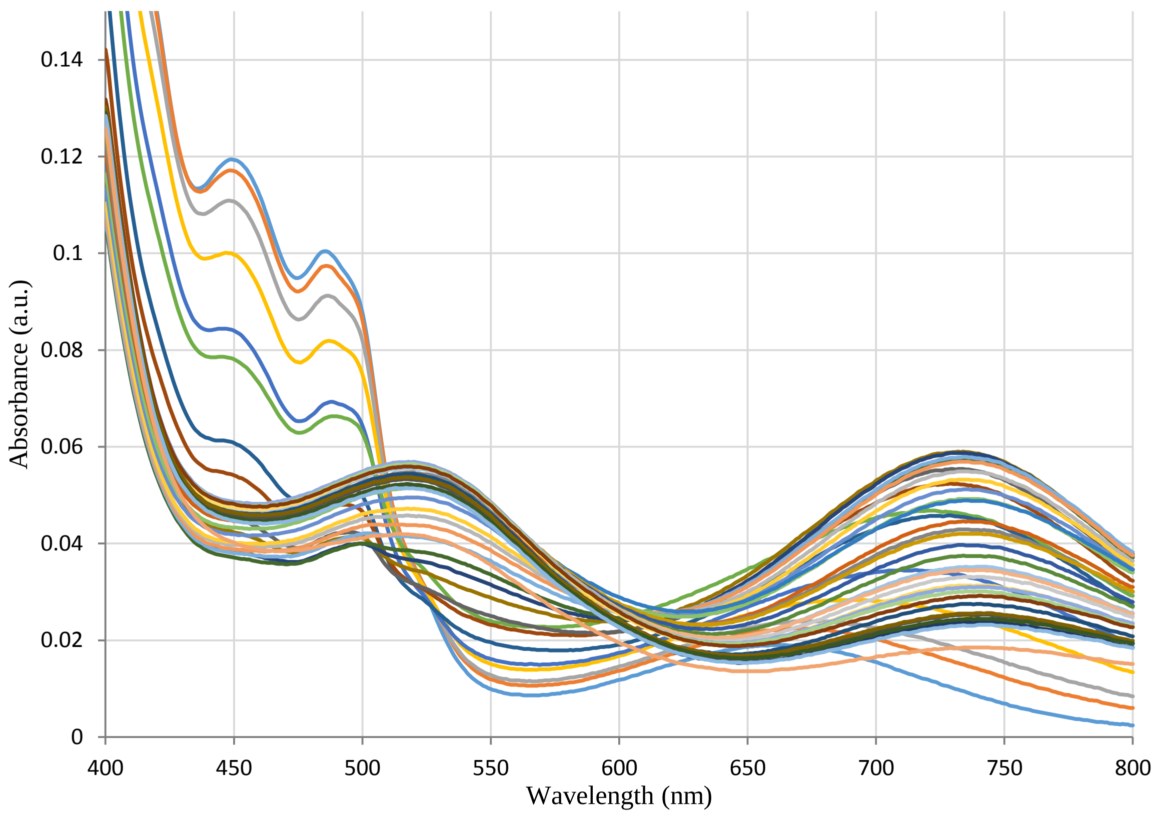

Figure S12. Visible spectra of a 145 µM solution of **1** titrated with 9.75 mM $NaIO_4$, a total of 12 equivalents of periodate (24 oxidizing equivalents) were added.

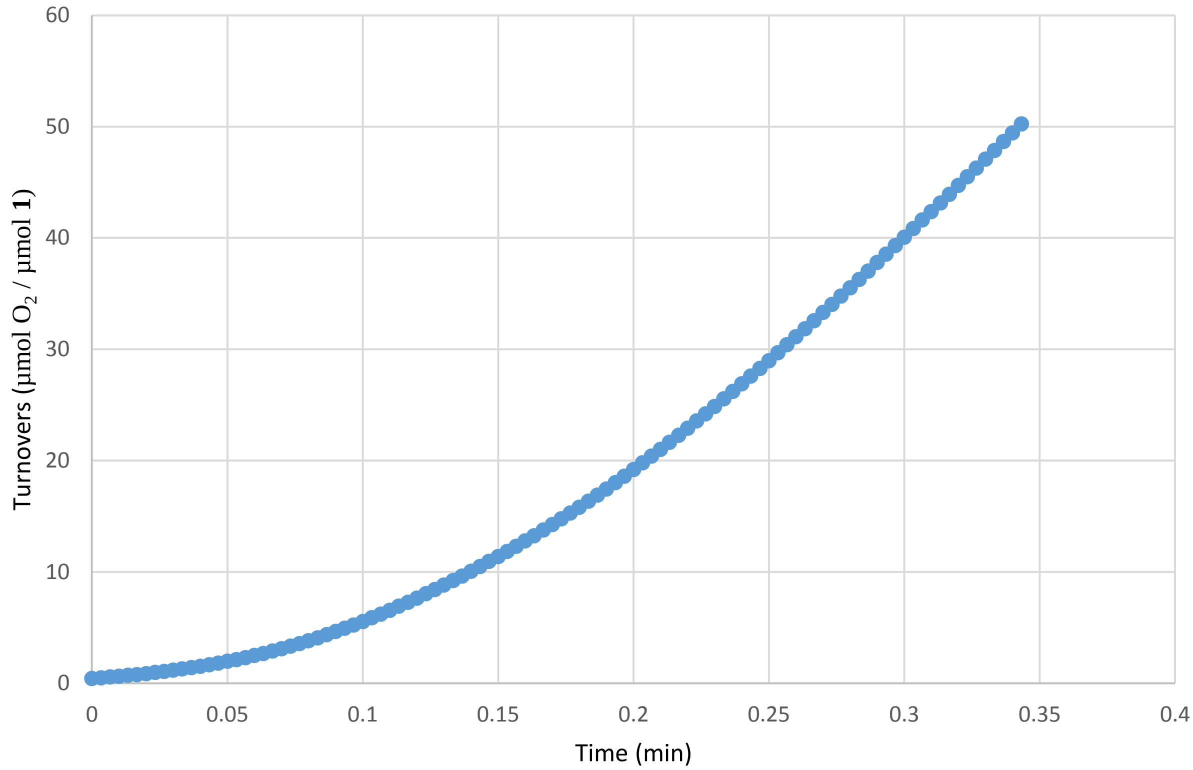

Figure S13. Turnovers vs. time for oxygen produced during the reaction of 12.4 µM **1** with 9.76 mM H_2O_2.

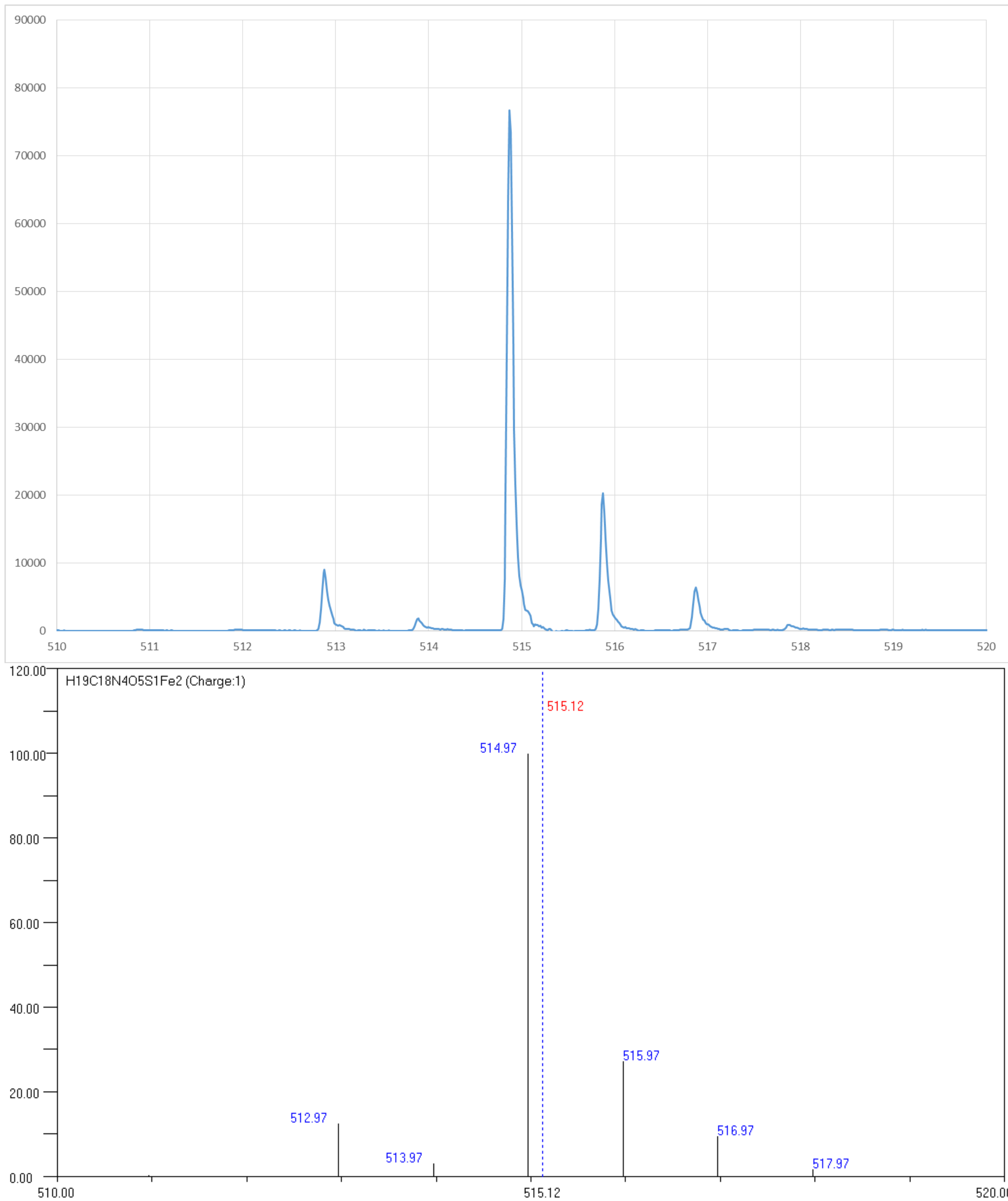

Figure S14. Observed (top) and calculated (bottom) isotope ratios for the peak at 514.9 m/z and its assigned species in Fig. 13a.

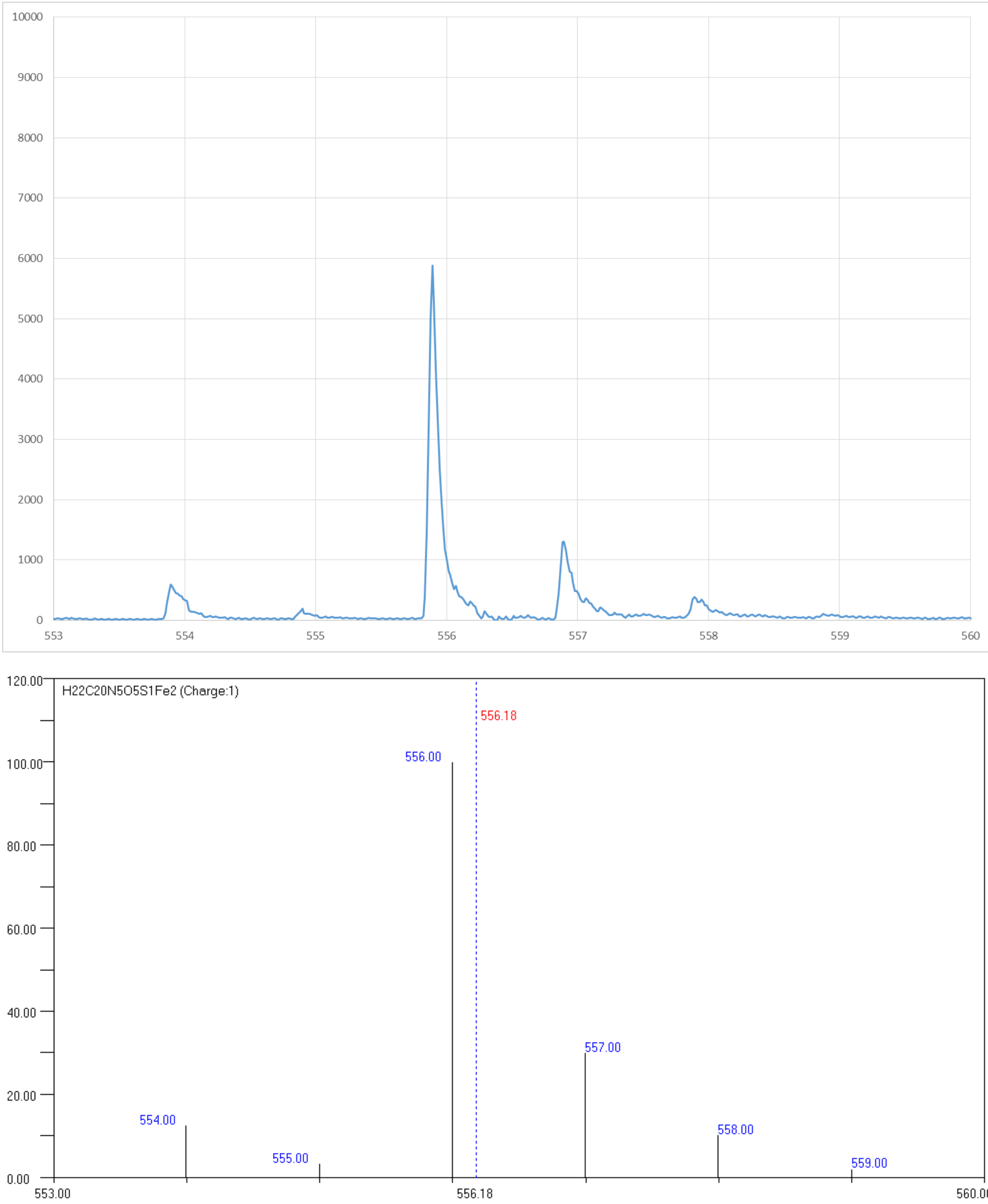

Figure S15. Observed (top) and calculated (bottom) isotope ratios for the peak at 555.9 m/z and its assigned species in Fig. 13b.

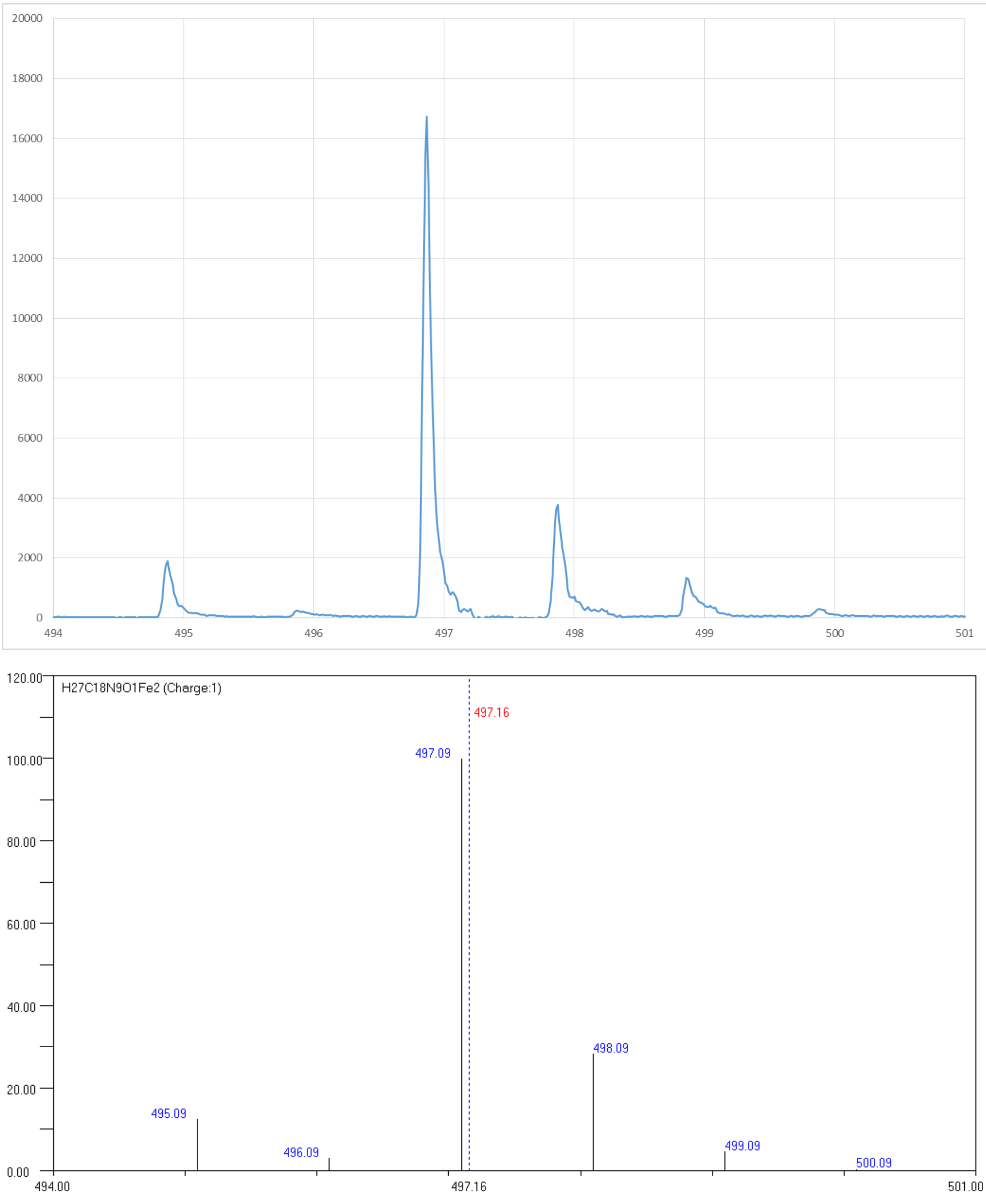

Figure S16. Observed (top) and calculated (bottom) isotope ratios for the peak at 496.9 m/z and its assigned species in Fig. 13c.

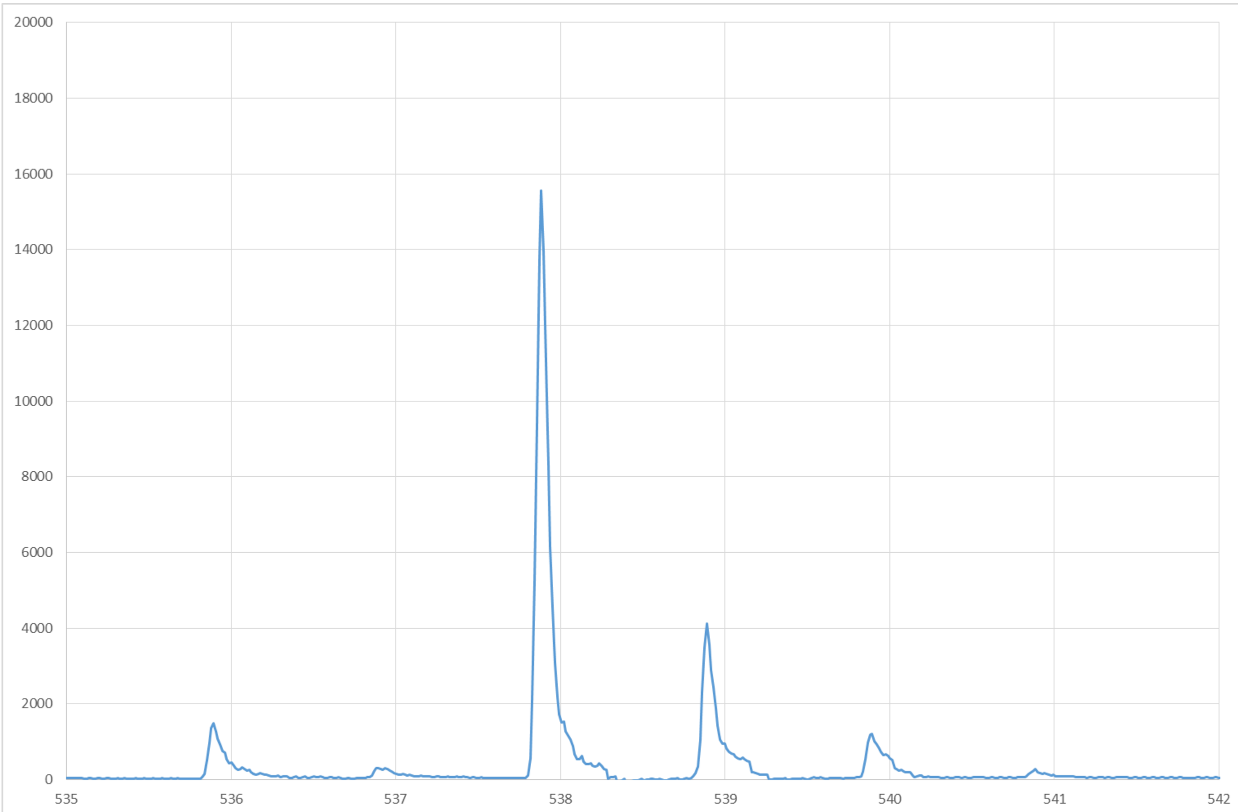

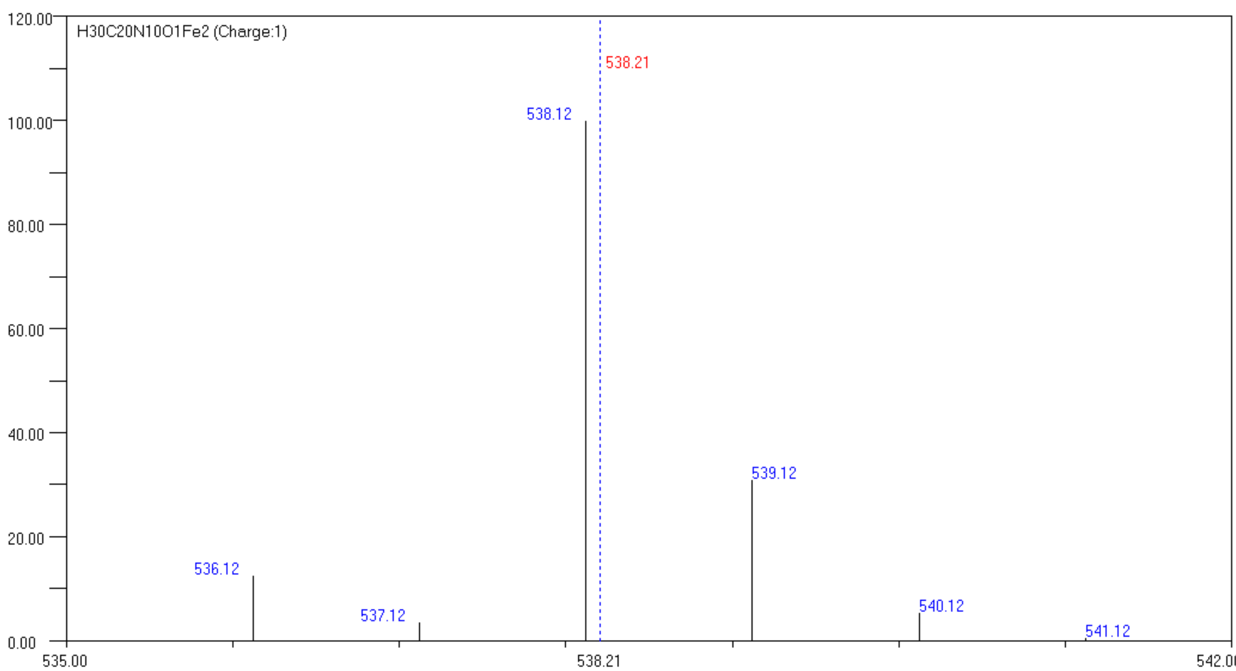

Figure S17. Observed (top) and calculated (bottom) isotope ratios for the peak at 537.9 m/z and its assigned species in Fig. 13d.

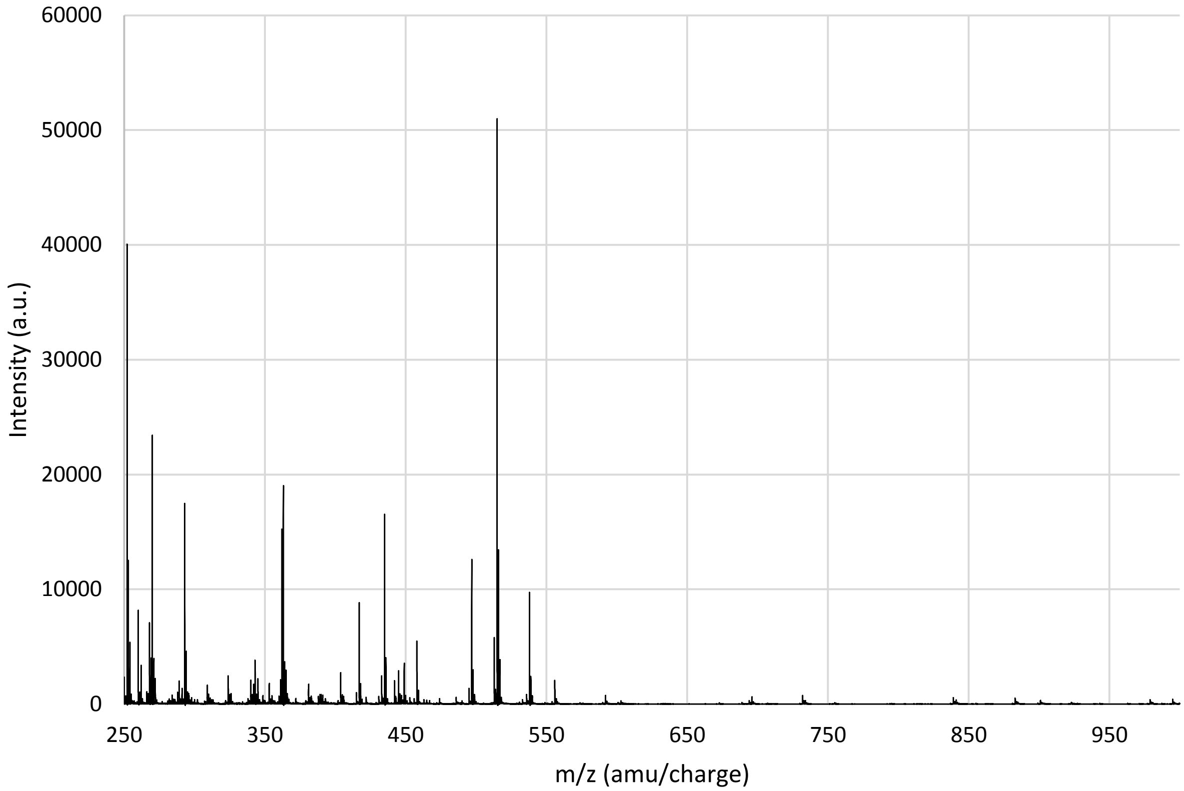

Figure S18. ESI-MS of **1** after dissolution in water, addition of 1 equivalent of sodium periodate, and dilution with acetonitrile.

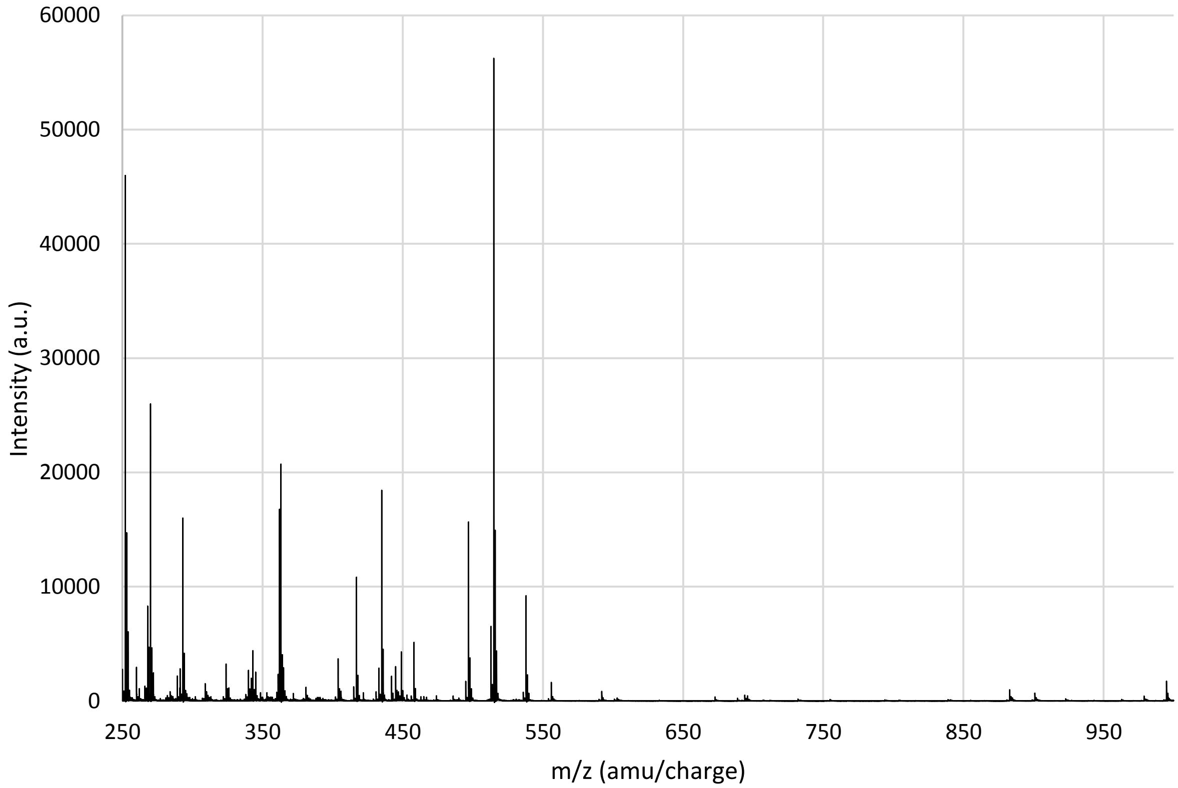

Figure S19. ESI-MS of **1** after dissolution in water, addition of 2 equivalents of sodium periodate, and dilution with acetonitrile.

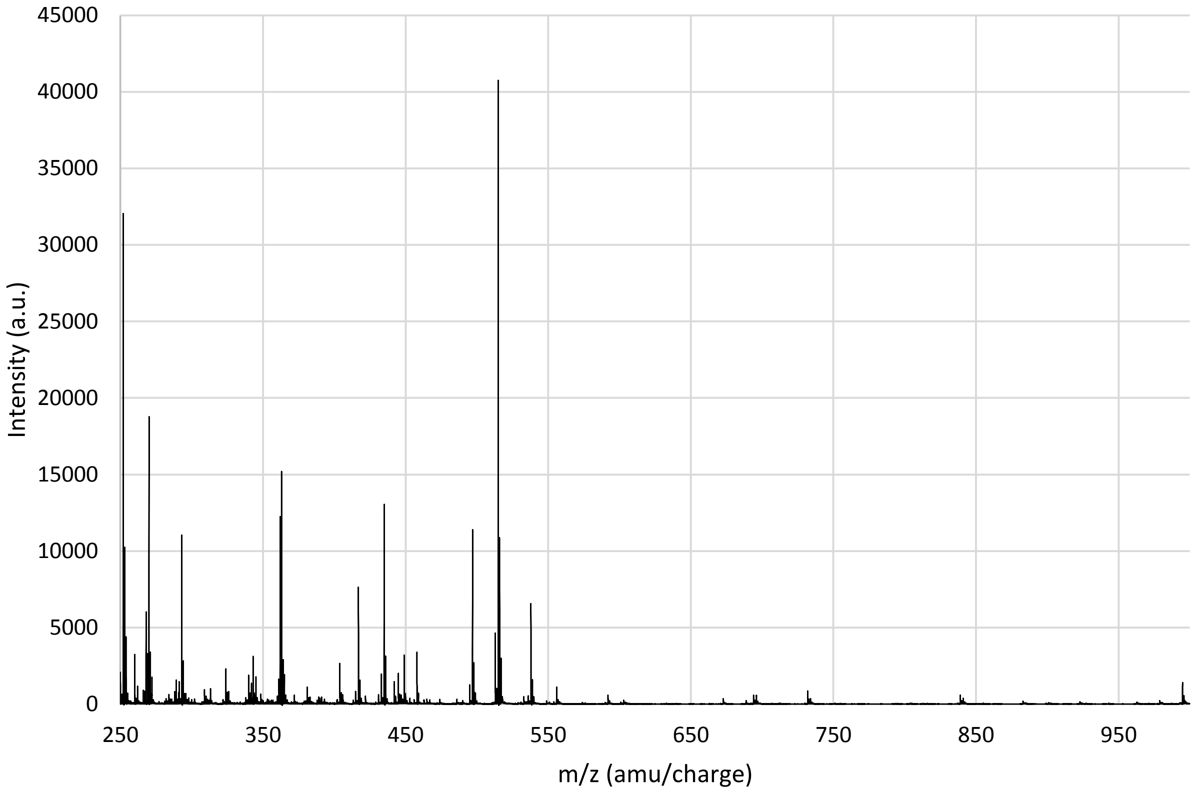

Figure S20. ESI-MS of **1** after dissolution in water, addition of 3 equivalents of sodium periodate, and dilution with acetonitrile.

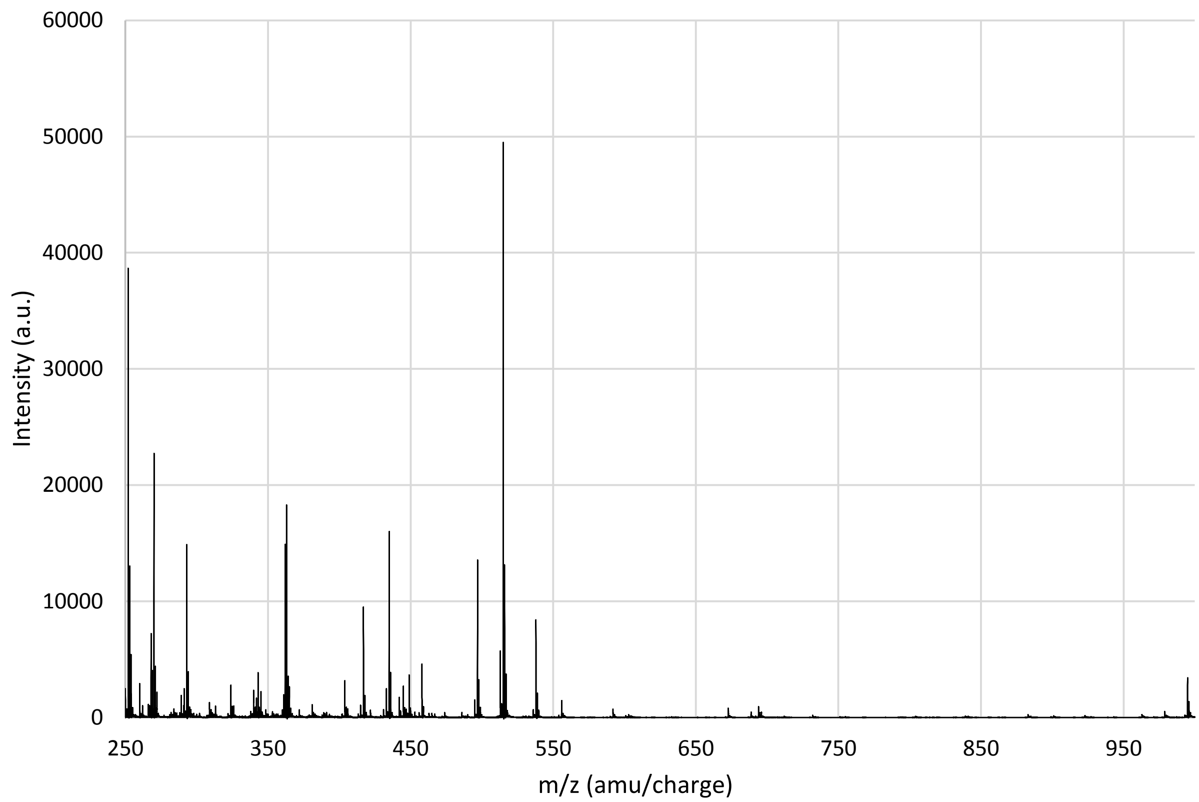

Figure S21. ESI-MS of **1** after dissolution in water, addition of 4 equivalents of sodium periodate, and dilution with acetonitrile.

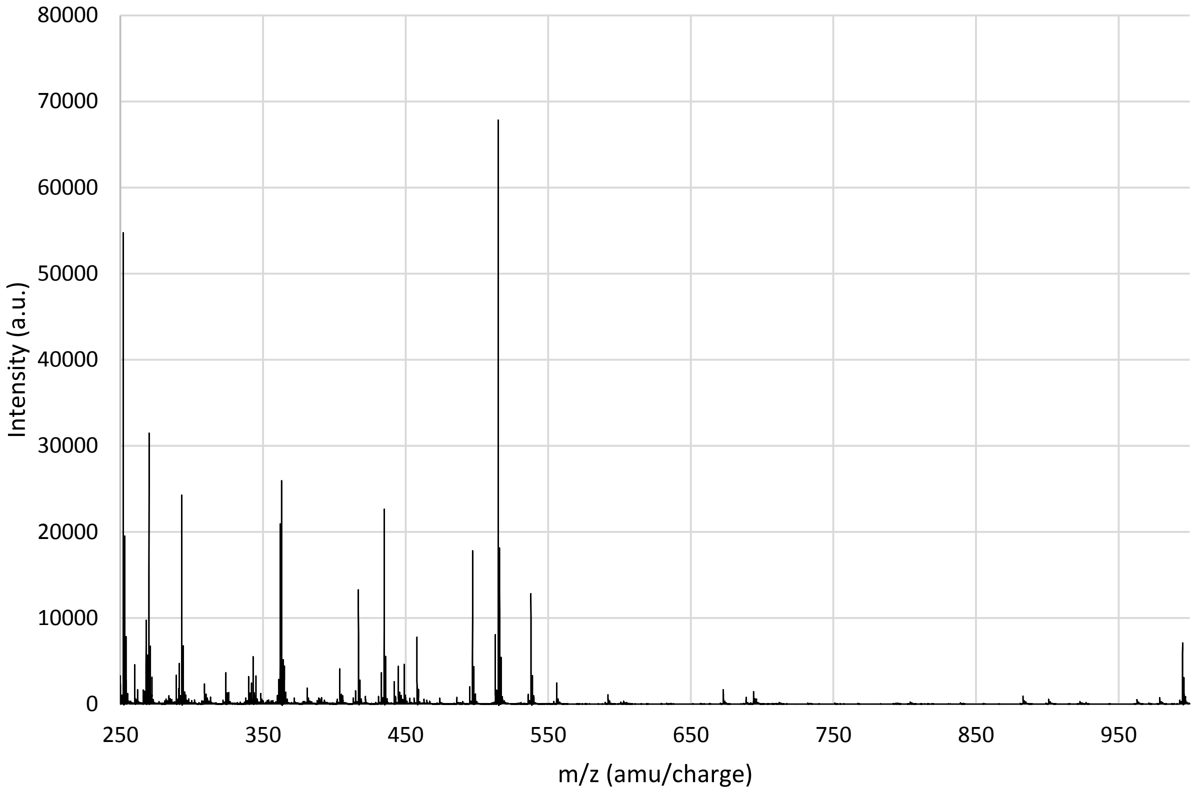

Figure S22. ESI-MS of **1** after dissolution in water, addition of 5 equivalents of sodium periodate, and dilution with acetonitrile.

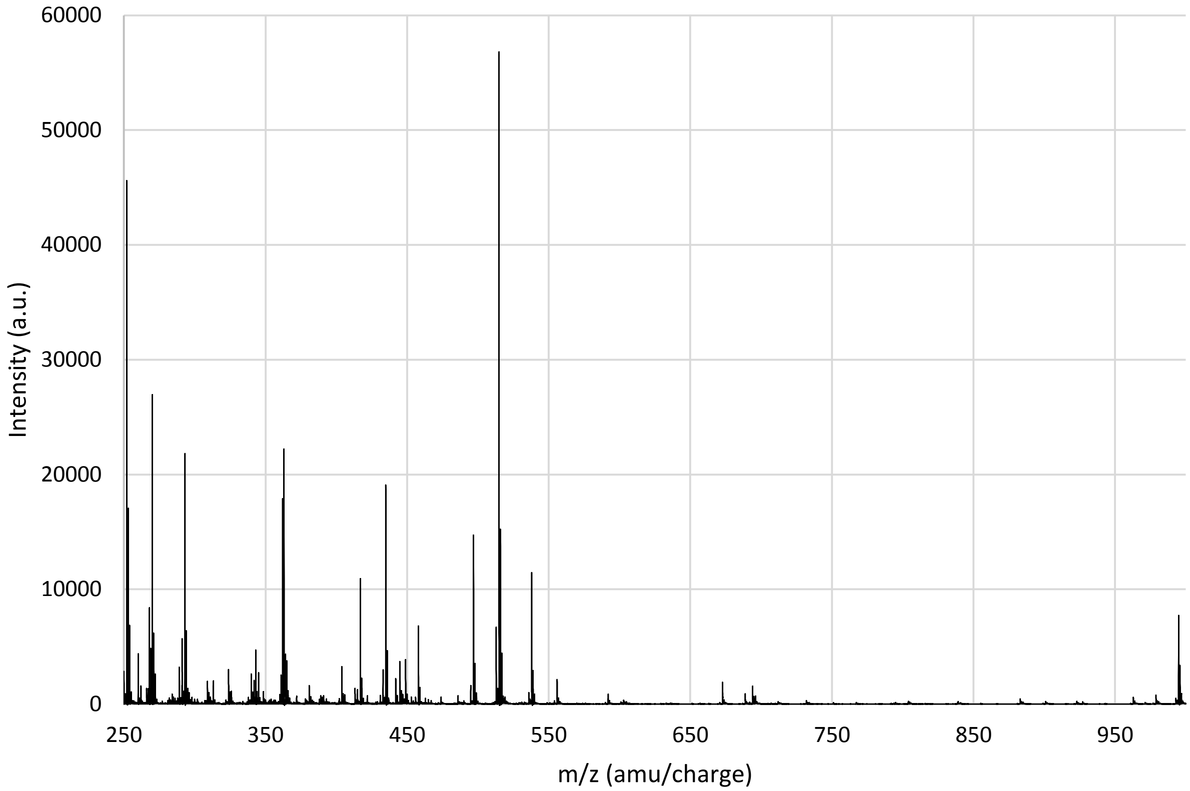

Figure S23. ESI-MS of **1** after dissolution in water, addition of 6 equivalents of sodium periodate, and dilution with acetonitrile.

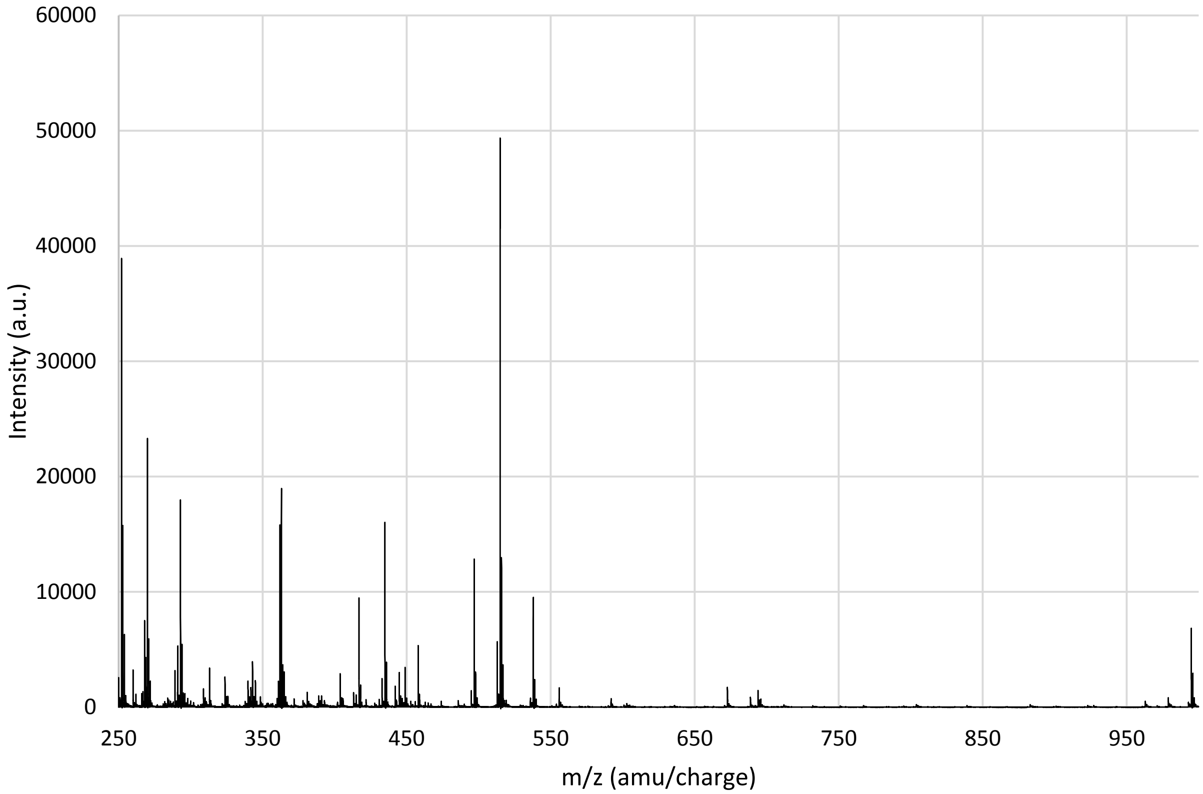

Figure S24. ESI-MS of **1** after dissolution in water, addition of 7 equivalents of sodium periodate, and dilution with acetonitrile.

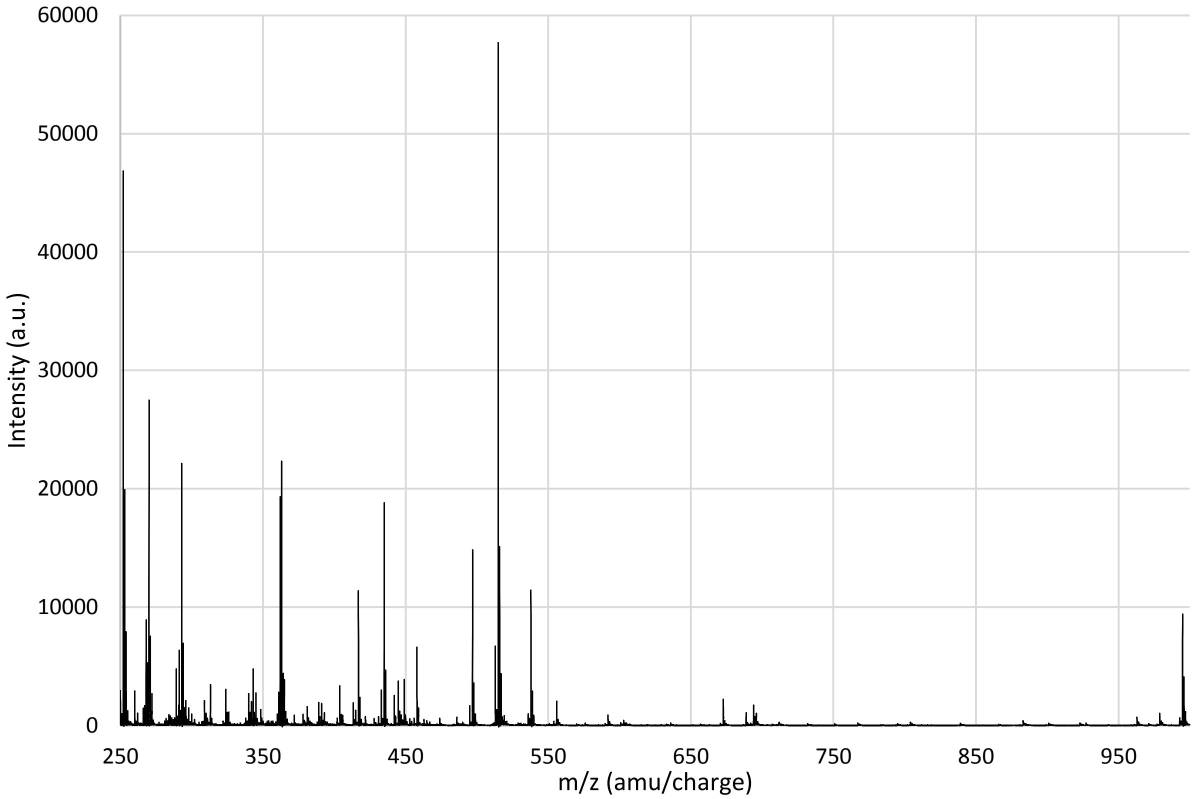

Figure S25. ESI-MS of **1** after dissolution in water, addition of 8 equivalents of sodium periodate, and dilution with acetonitrile.

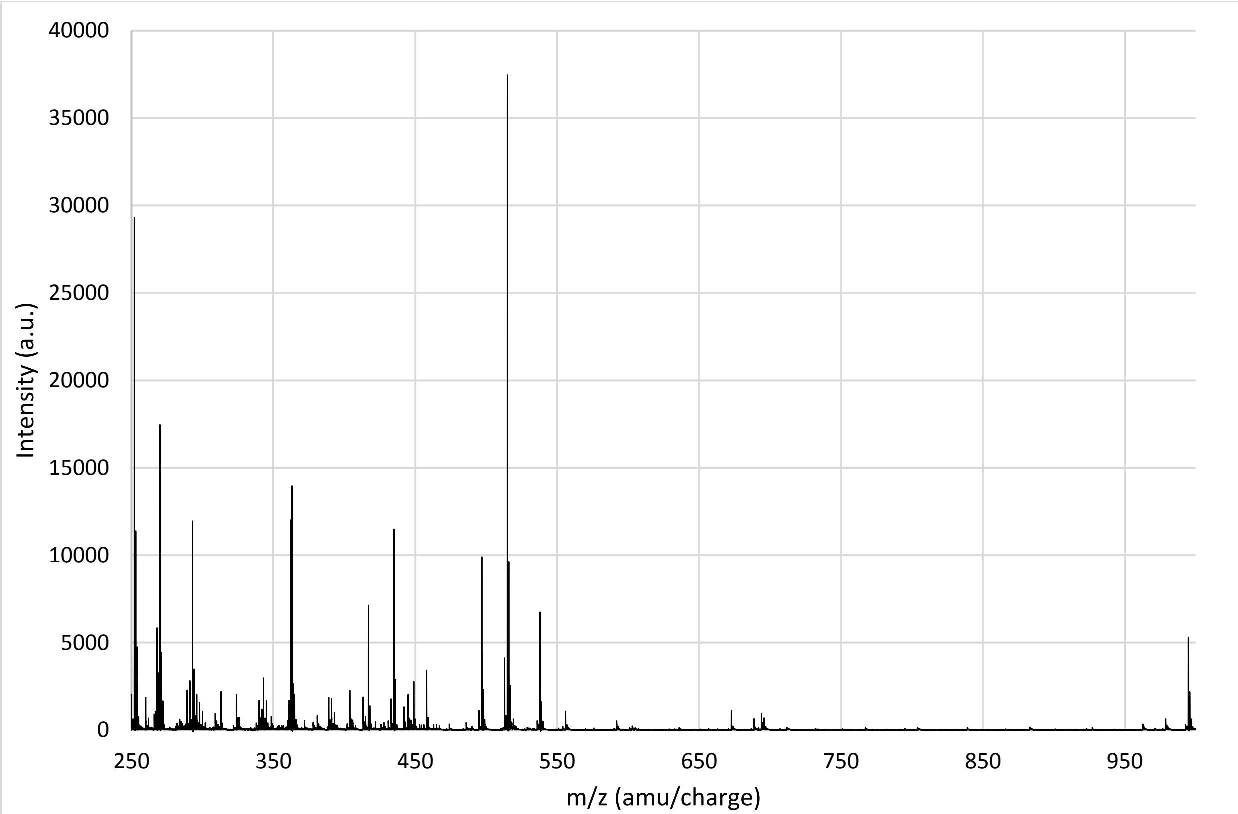

Figure S26. ESI-MS of **1** after dissolution in water, addition of 9 equivalents of sodium periodate, and dilution with acetonitrile.

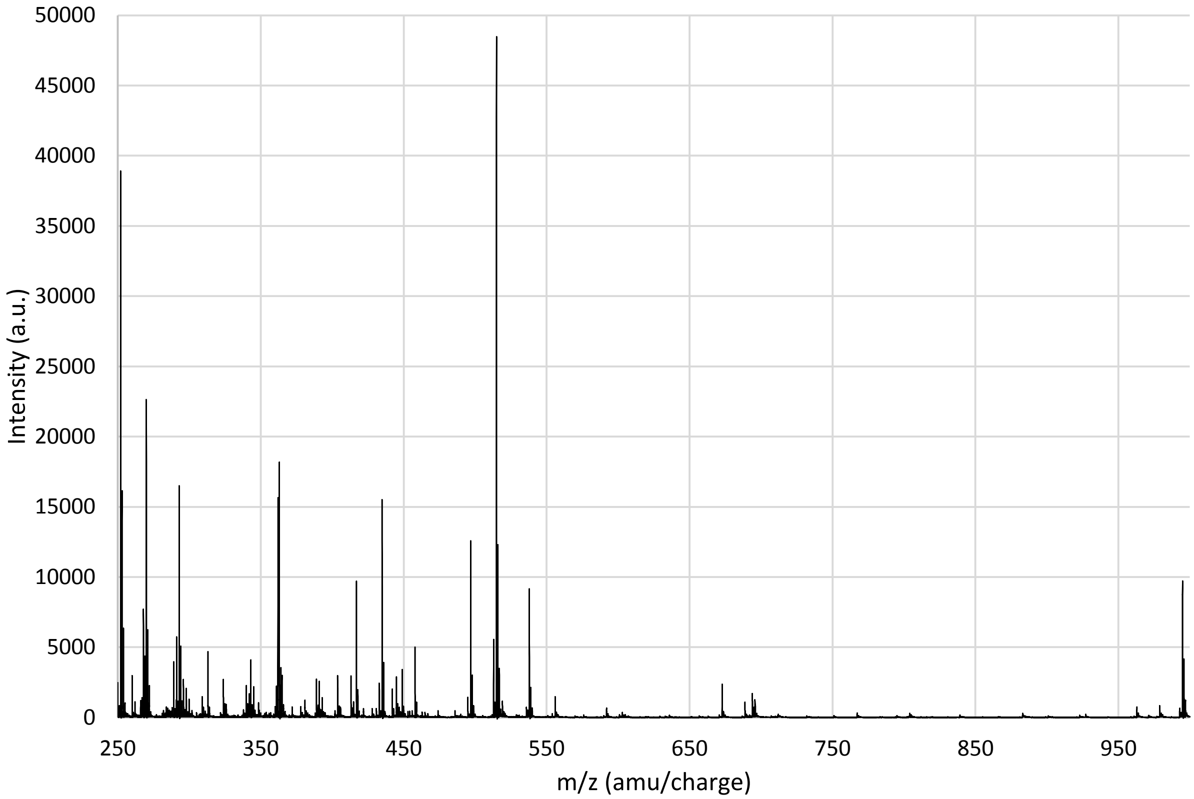

Figure S27. ESI-MS of **1** after dissolution in water, addition of 10 equivalents of sodium periodate, and dilution with acetonitrile.

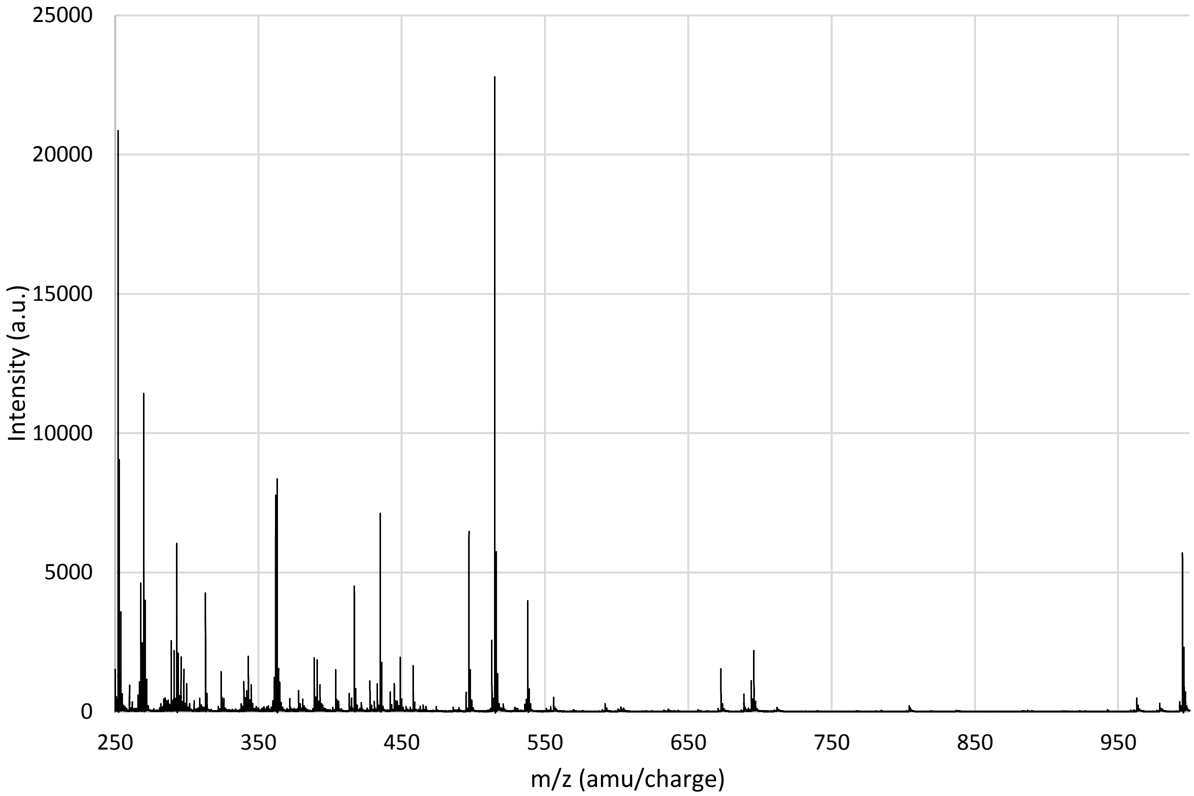

Figure S28. ESI-MS of **1** after dissolution in water, addition of 14 equivalents of sodium periodate, and dilution with acetonitrile.

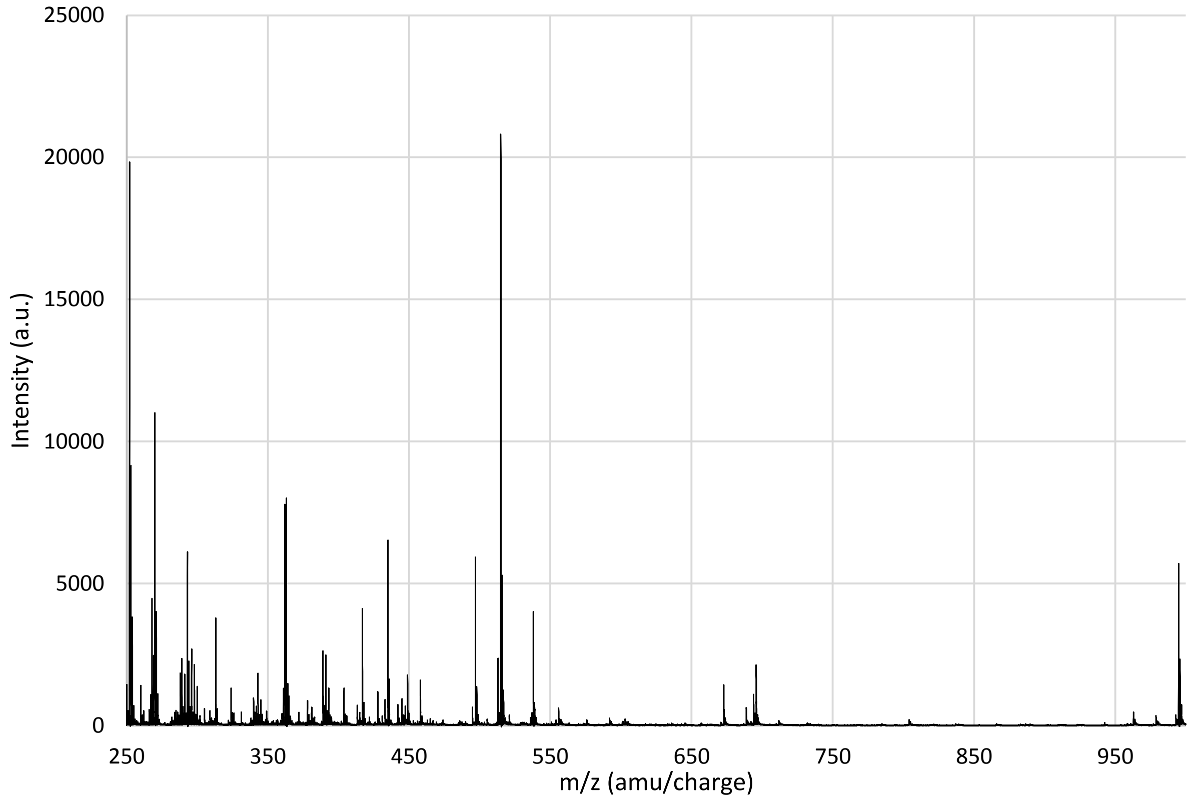

Figure S29. ESI-MS of **1** after dissolution in water, addition of 16 equivalents of sodium periodate, and dilution with acetonitrile.

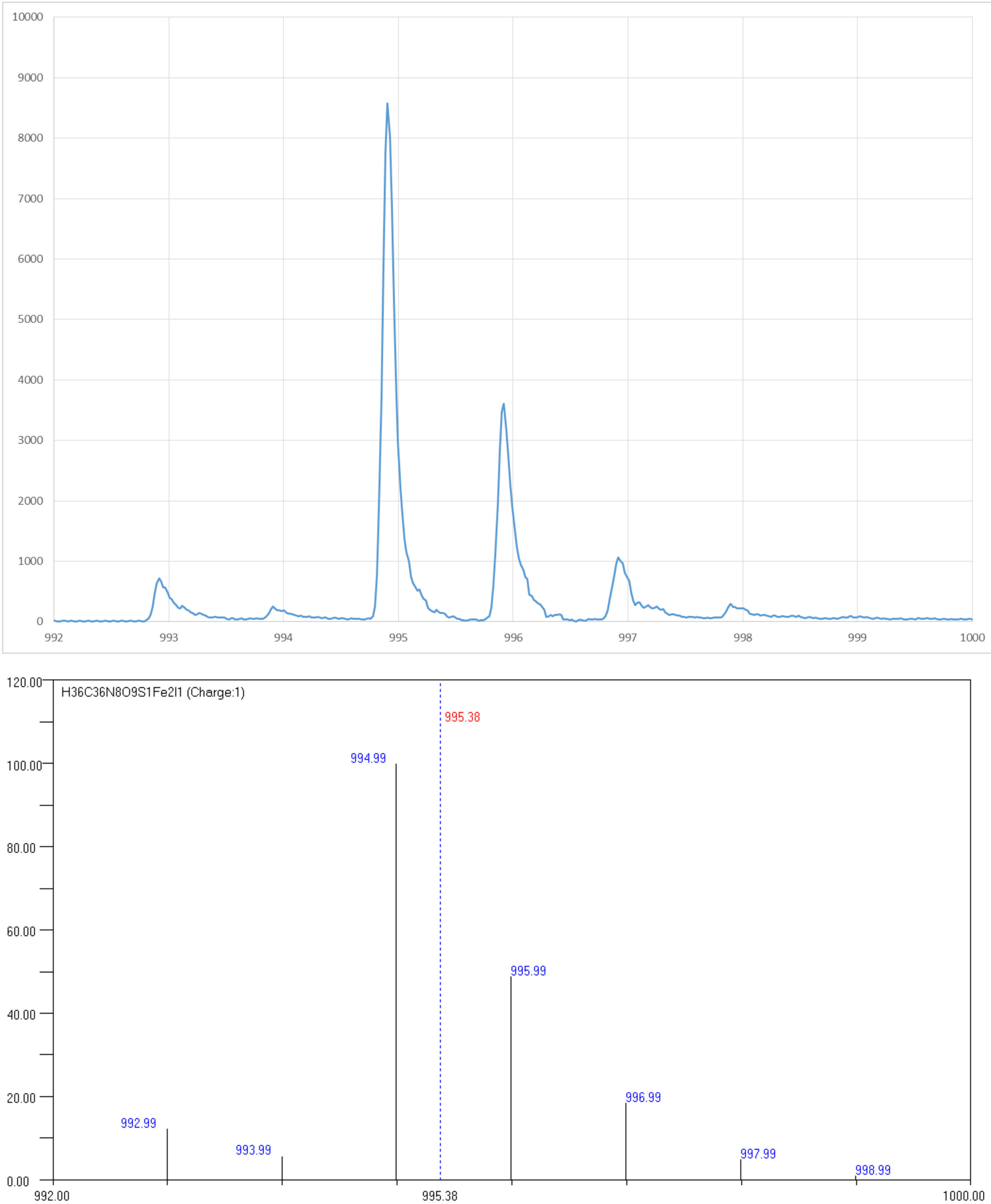

Figure S30. Observed (top) and calculated (bottom) isotope ratios for the peak at 994.9 m/z and its assigned species in Fig. 13e.

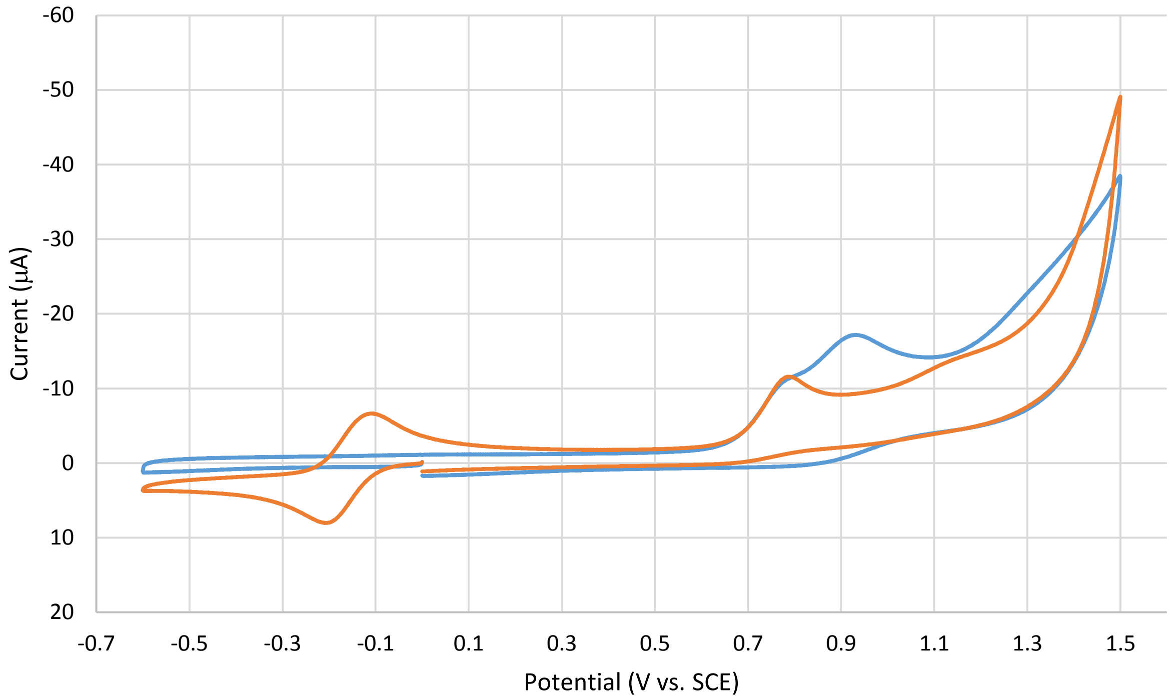

Figure S31. Cyclic voltammogram of 0.5 mM **2** (orange) and 1.0 mM BPyA (blue), under Ar purge in 100 mM aqueous phosphate buffer, pH 6.8. The peak at ~0.78 V vs. SCE in **2** appears to correspond to ligand oxidation. Further oxidation of the ligand which occurs at ~0.92 V vs. SCE appears to be inhibited by coordination to Fe.

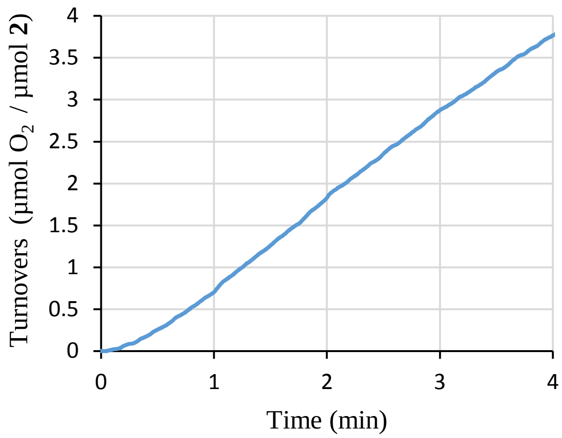

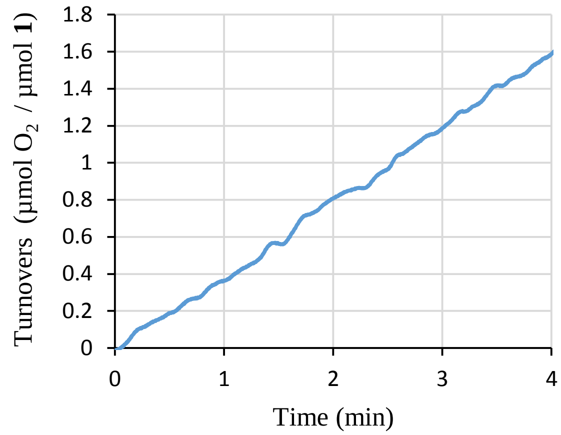

Figure S32. Turnovers vs. time for the reaction of 10.6 µM **2** with 10.1 mM $NaIO_4$ (left), and for the reaction of 12.4 µM **1** with 10.0 mM $NaIO_4$ (right).

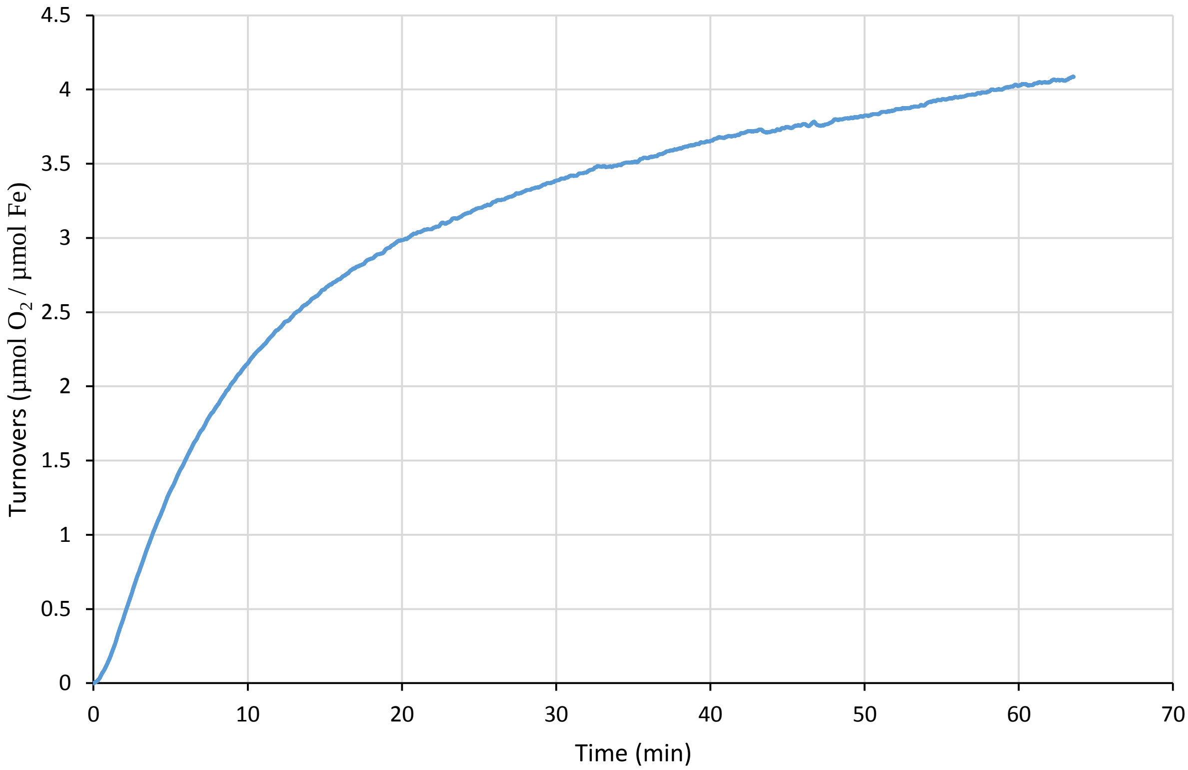

Figure S33. Turnovers vs. time for the reaction of 51.9 µM **2** (Fe basis) with 10.0 mM sodium periodate.

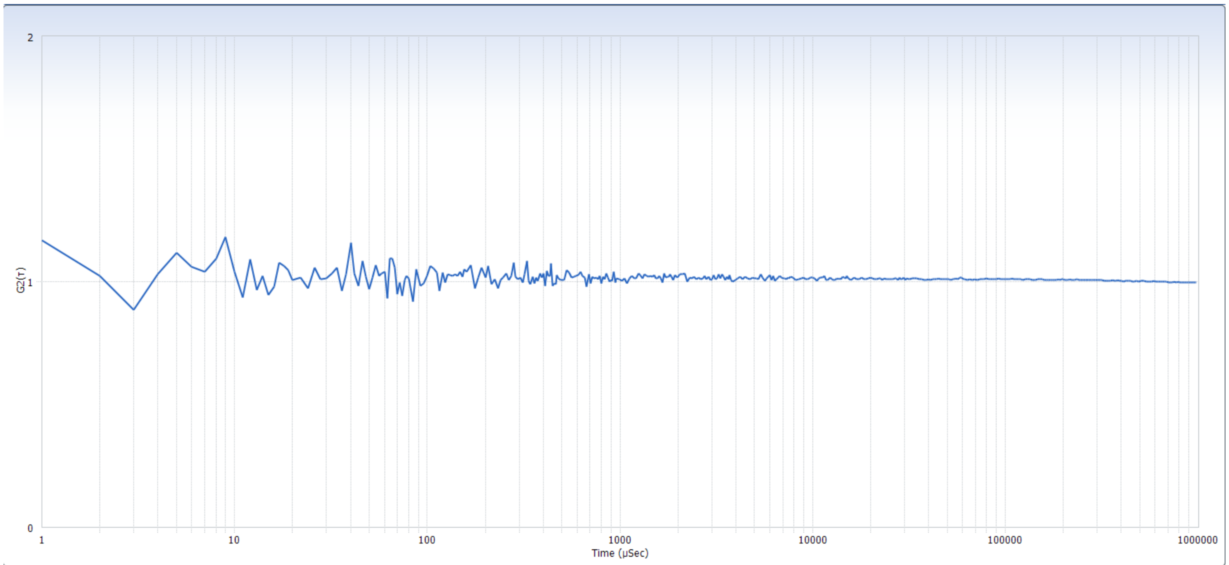

Figure S34. ACF fitting curve of a solution of 0.92 mM $NaIO_4$.

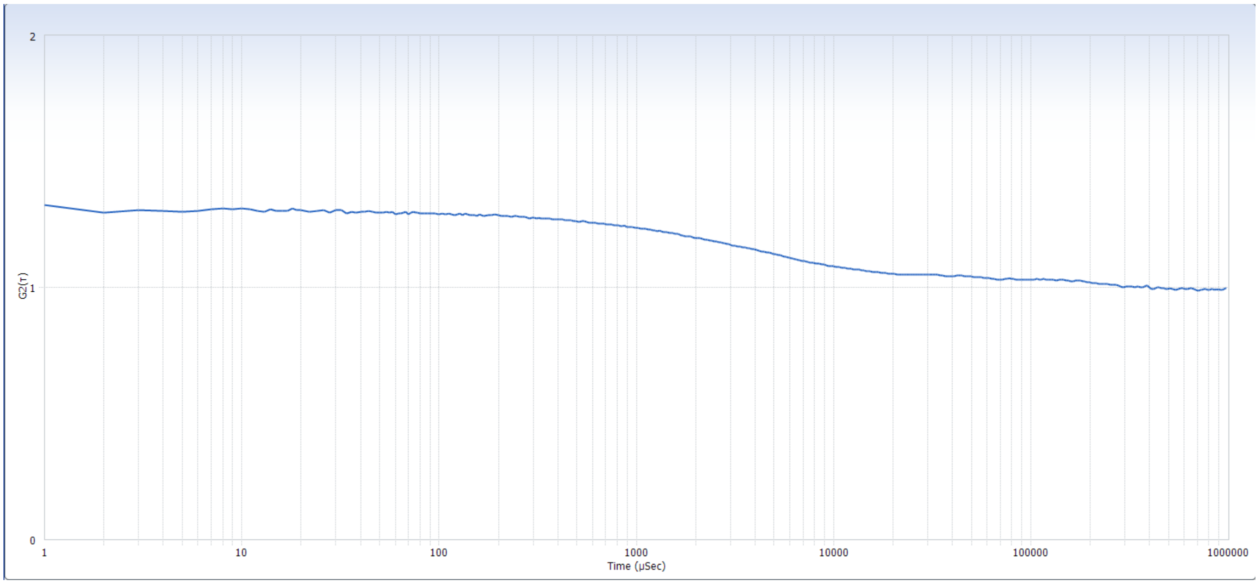

Figure S35. ACF fitting curve after addition of 84.7μM $Fe(NO_3)_3$ to 0.92 mM $NaIO_4$.

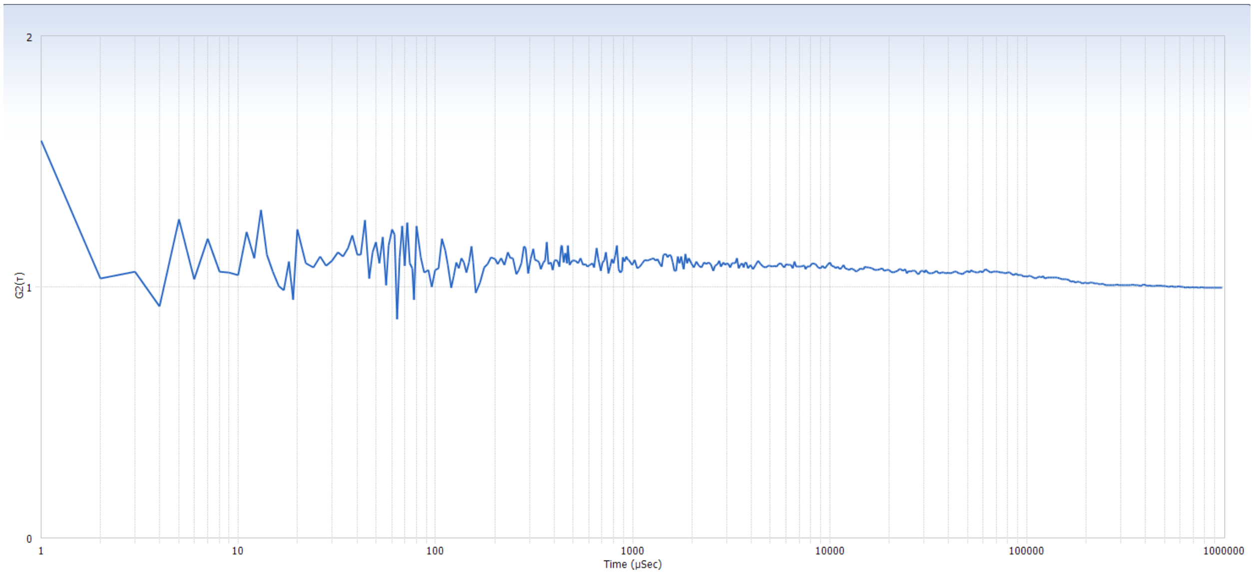

Figure S36. ACF fitting curve of 10 mM $NaIO_4$.

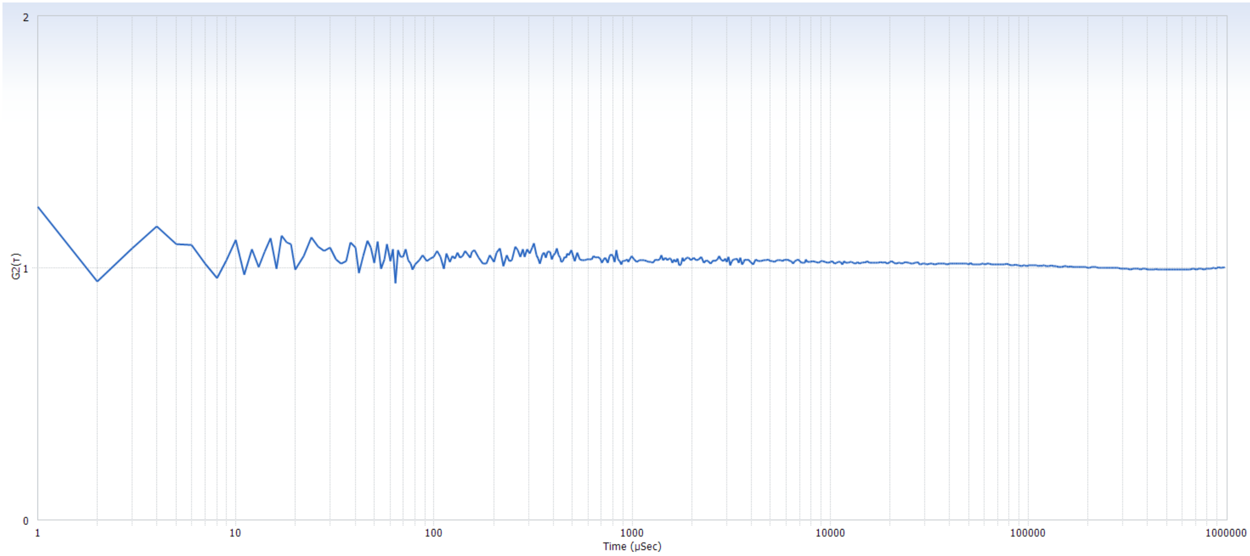

Figure S37. ACF fitting curve 4 minutes after addition of 30.7 µM **1** to 10 mM $NaIO_4$.

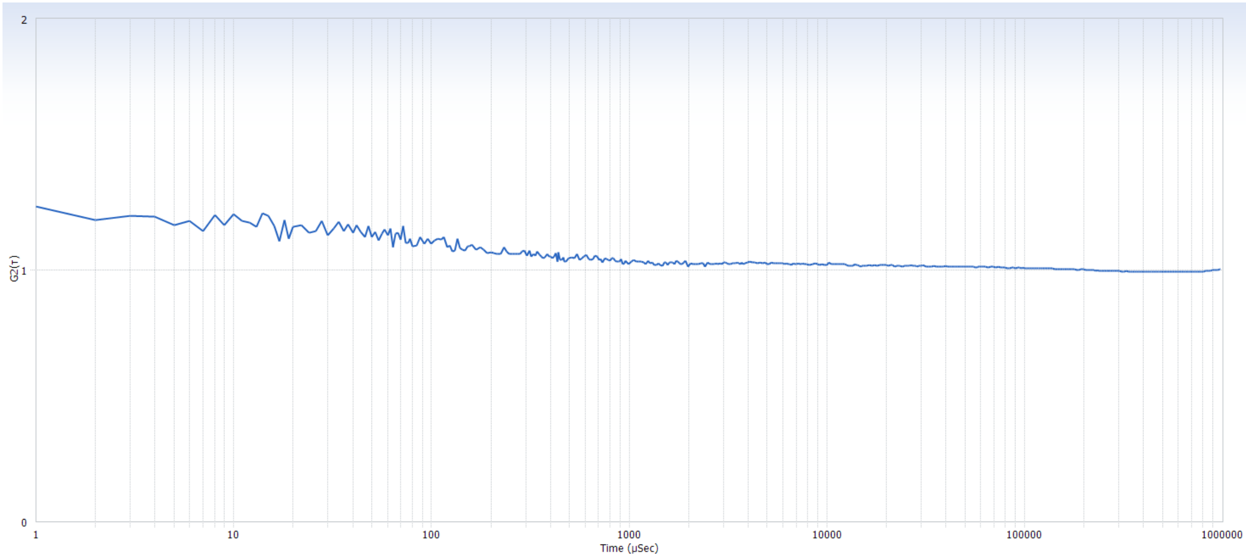

Figure S38. ACF fitting curve 80 minutes after addition of 30.7 μM **1** to 10 mM $NaIO_4$.

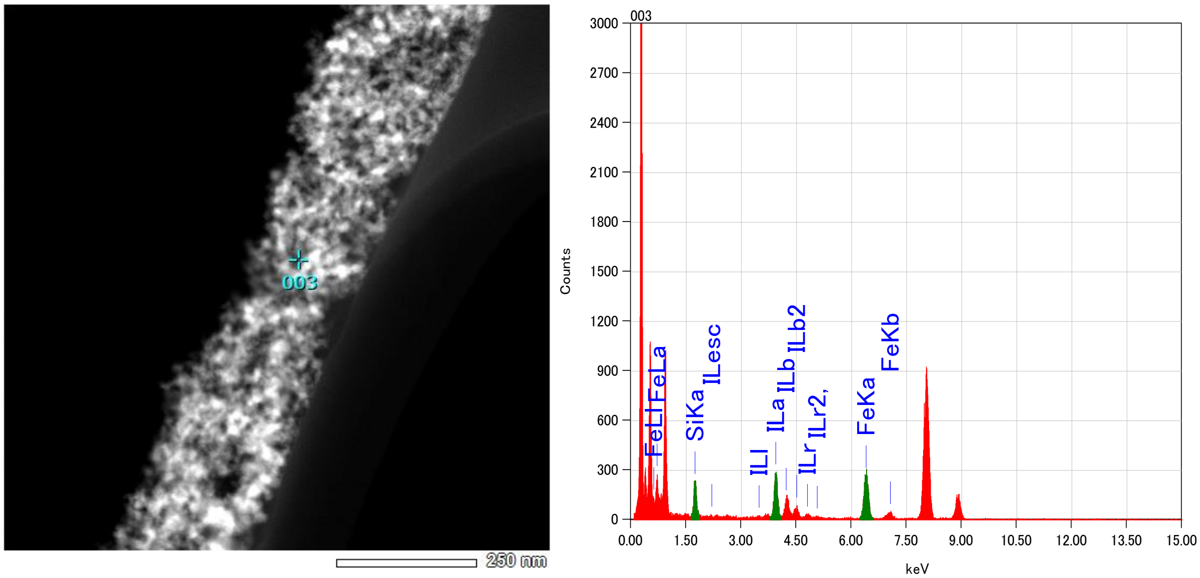

Figure S39. A high angle annular dark-field scanning TEM (HAADF-STEM) image (left) and the EDS point analysis (right) indicated by the cross in the left pane for nanoparticles generated during the reaction of $Fe(NO_3)_3$ with sodium periodate.

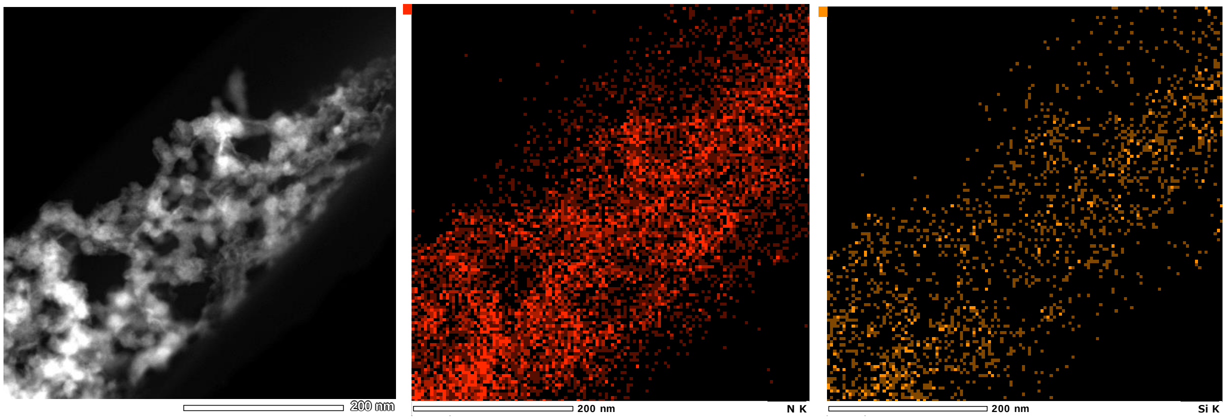

Figure S40. A HAADF-STEM image of nanoparticulate matter formed during the reaction of $Fe(NO_3)_3$ with sodium periodate (left) and the elemental map of N K-line (middle) and Si K-line (right). Compare with Fig. 18 in the main text.

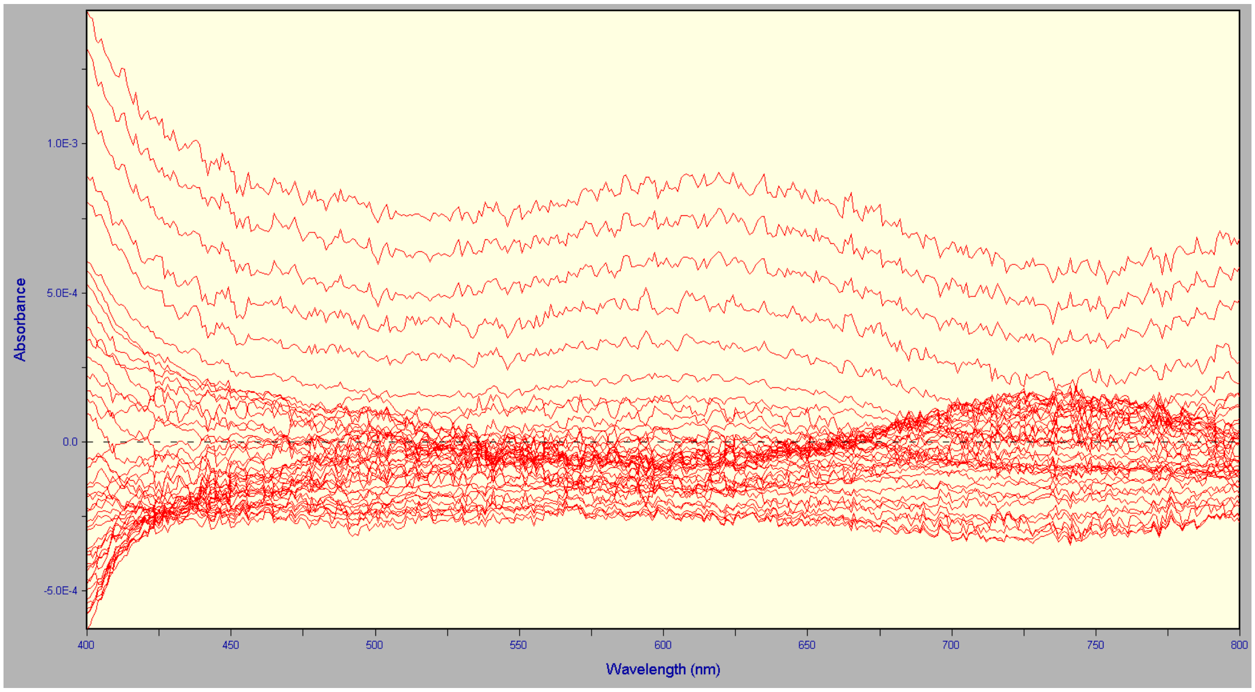

Figure S41. Residuals from the SPECFIT fitting of the reaction of 48.5 µM **1** with 10.0 mM sodium periodate.

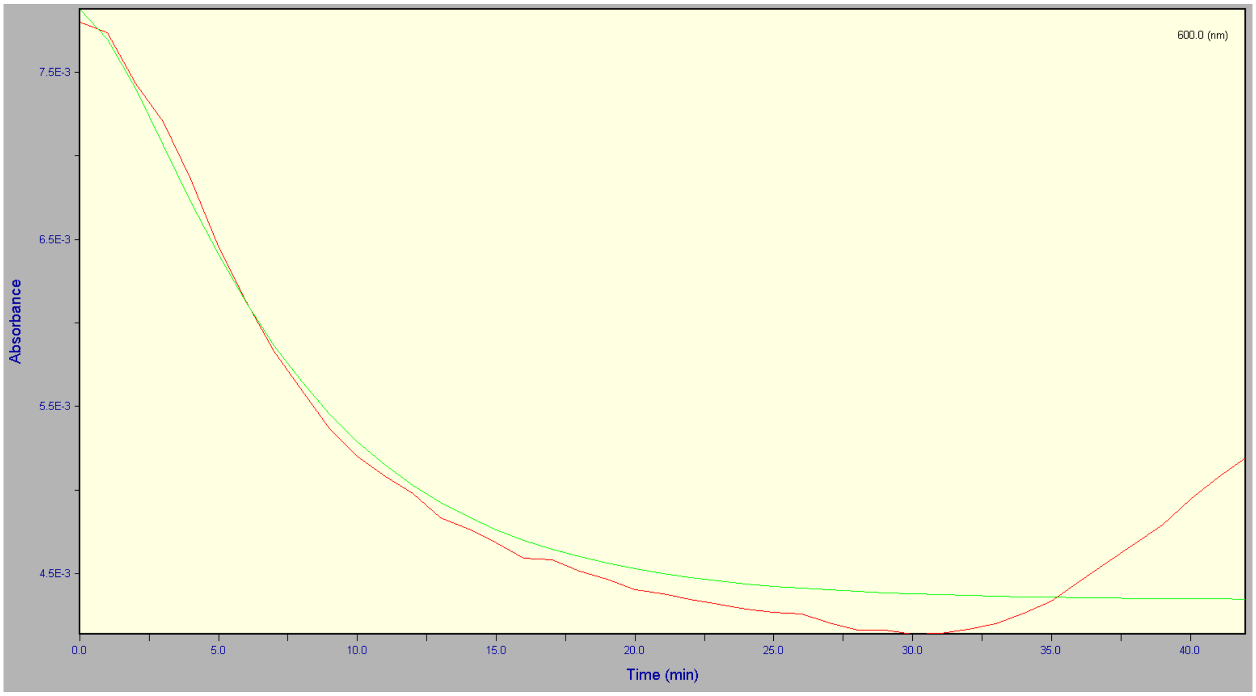

Figure S42. SPECFIT fitting of the reaction of 48.5 µM **1** with 10.0 mM sodium periodate (green) vs. the observed absorbance at 600 nm (red).

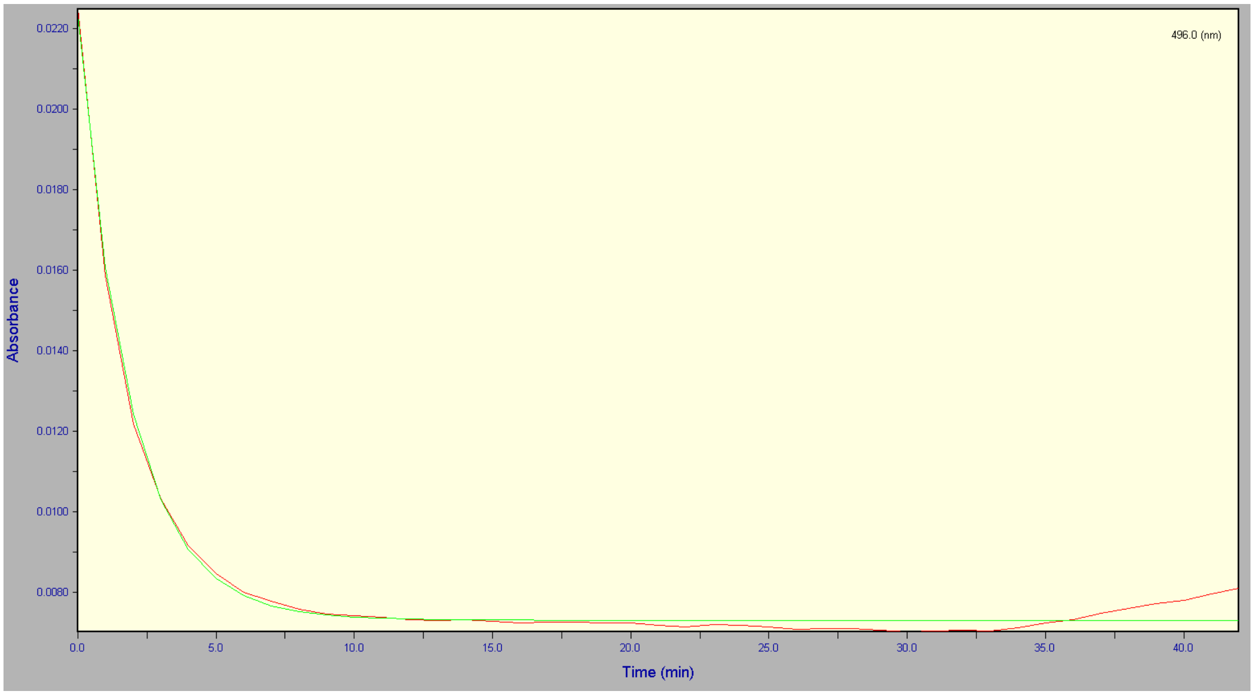

Figure S43. SPECFIT fitting of the reaction of 48.5 µM **1** with 10.0 mM sodium periodate (green) vs. the observed absorbance at 496 nm (red).

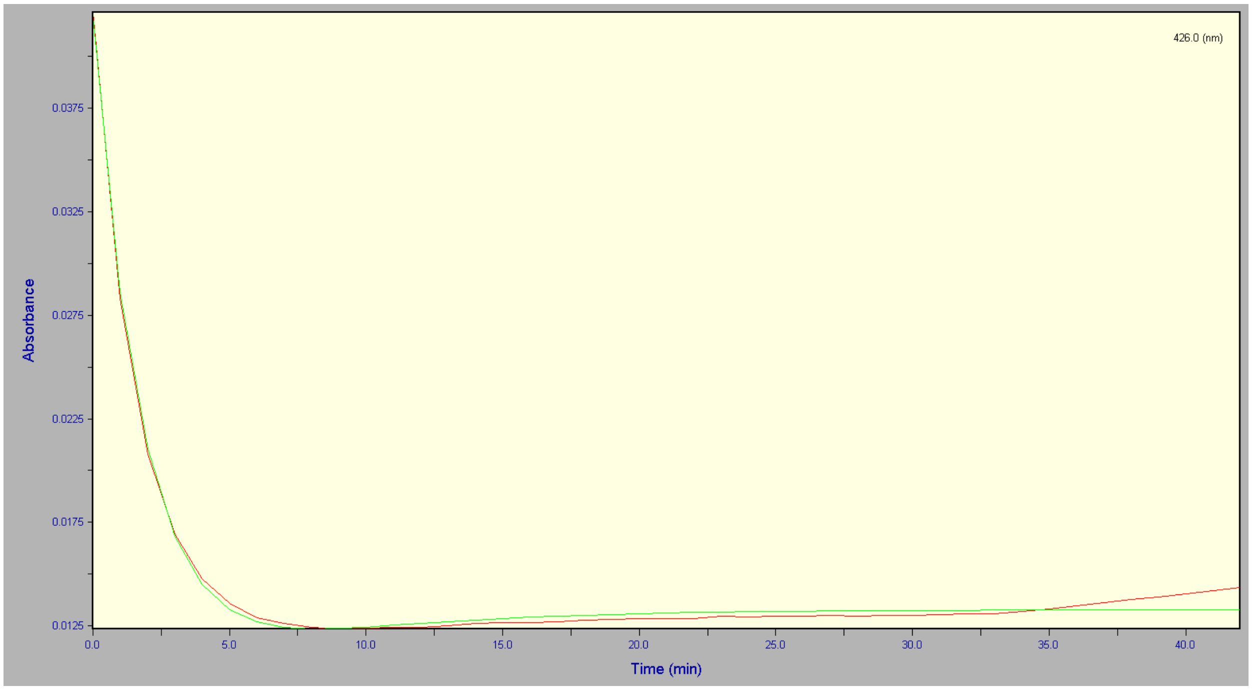

Figure S44. SPECFIT fitting of the reaction of 48.5 μM **1** with 10.0 mM sodium periodate (green) vs. the observed absorbance at 426 nm (red).

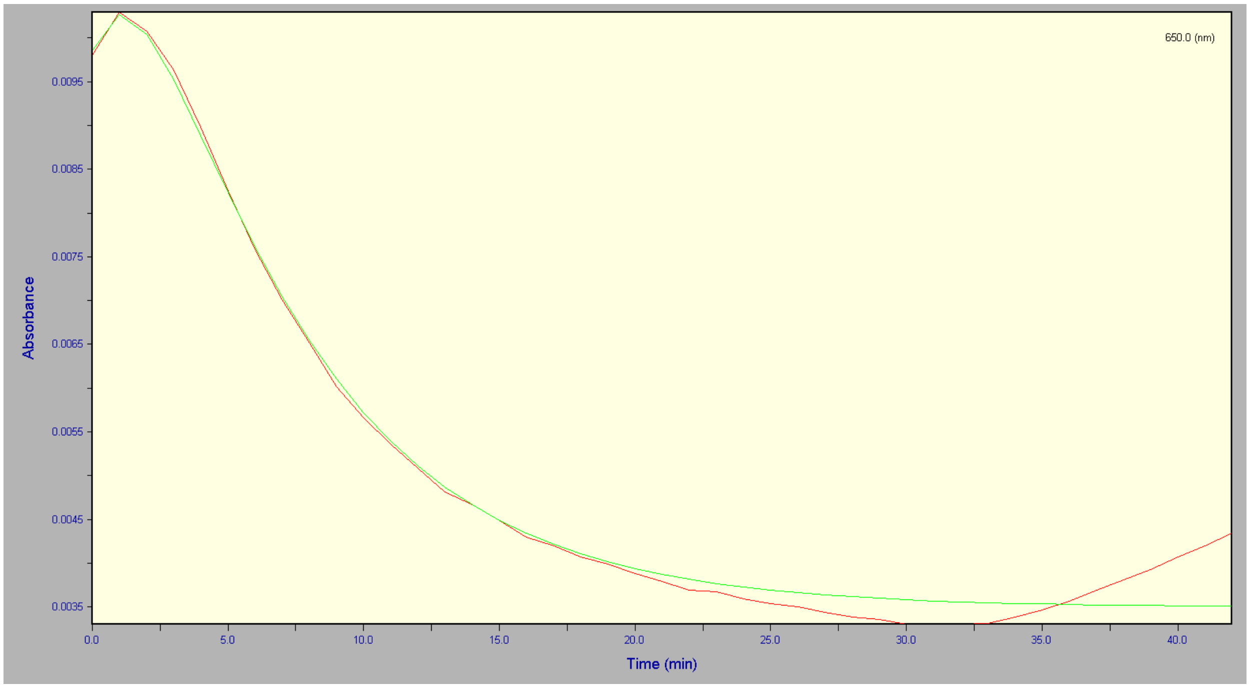

Figure S45. SPECFIT fitting of the reaction of 48.5 µM **1** with 10.0 mM sodium periodate (green) vs. the observed absorbance at 650 nm (red).

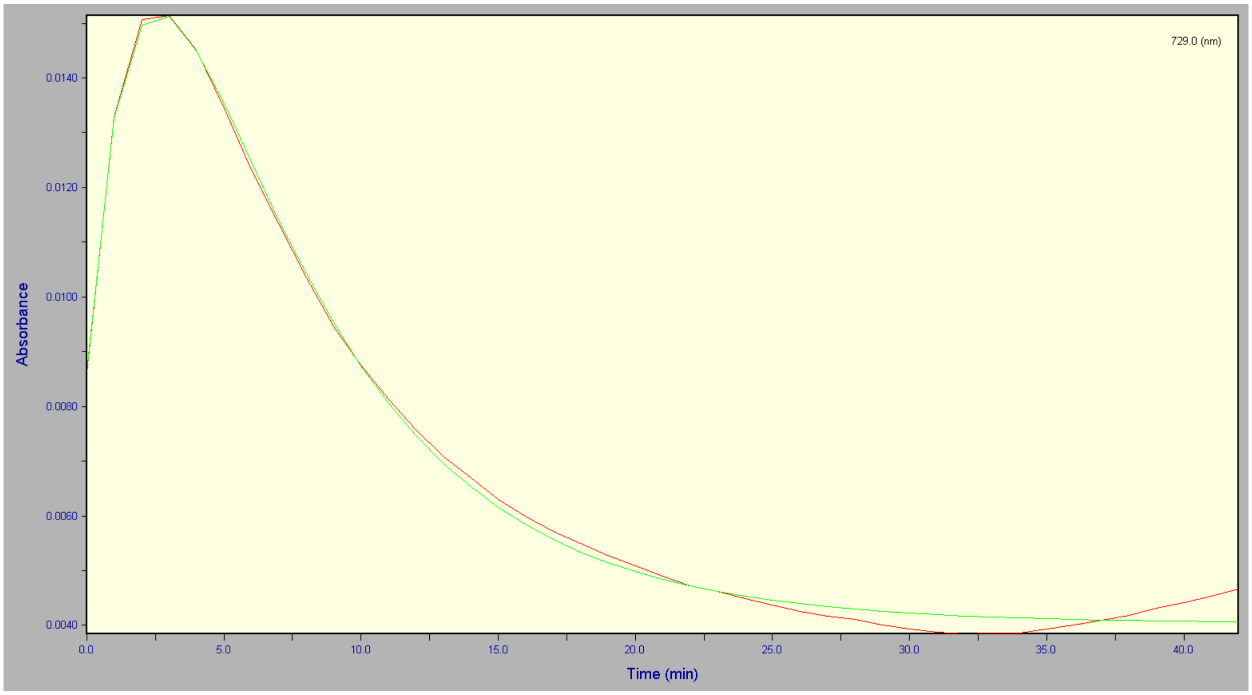

Figure S46. SPECFIT fitting of the reaction of 48.5 µM **1** with 10.0 mM sodium periodate (green) vs. the observed absorbance at 729 nm (red).

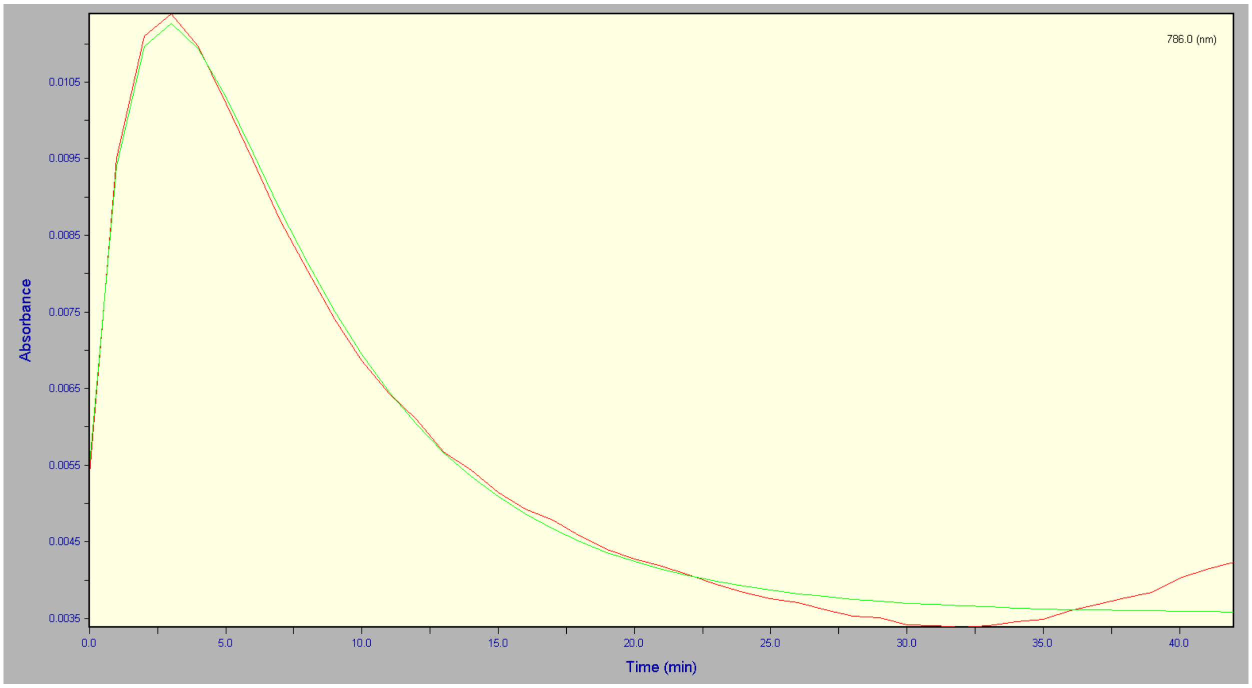

Figure S47. SPECFIT fitting of the reaction of 48.5 μM **1** with 10.0 mM sodium periodate (green) vs. the observed absorbance at 786 nm (red).

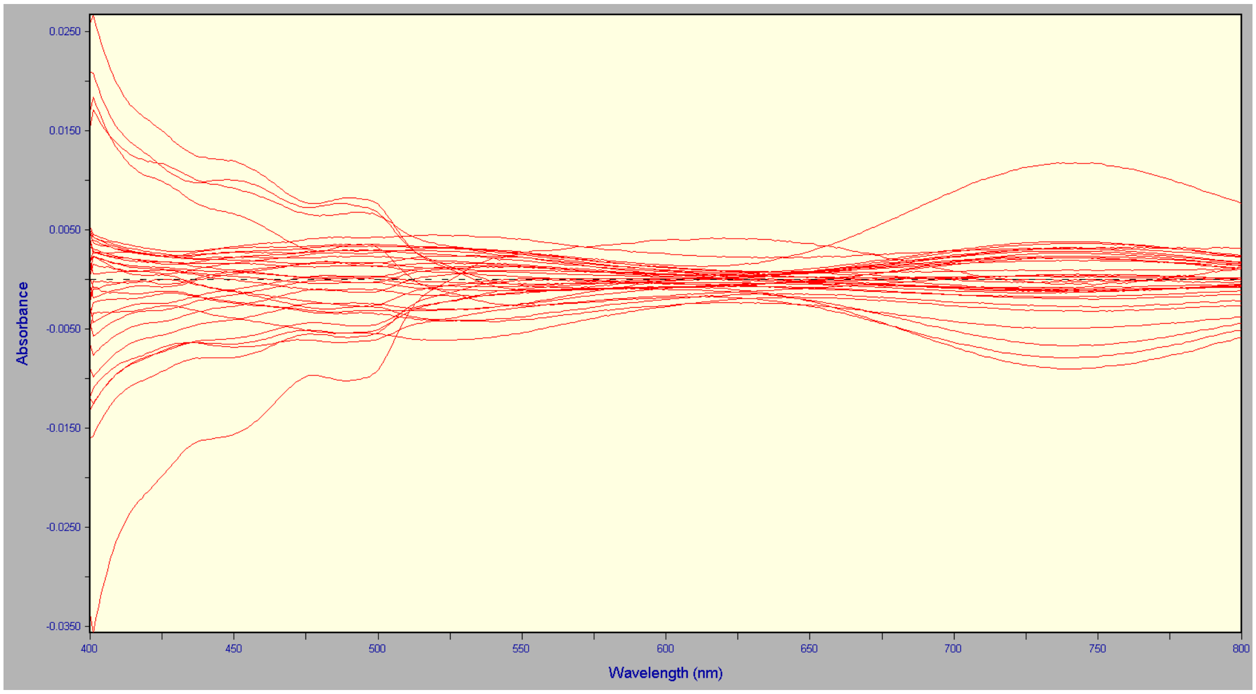

Figure S48. Residuals from the SPECFIT fitting of the titration of 145 µM **1** with 9.75 mM sodium periodate.

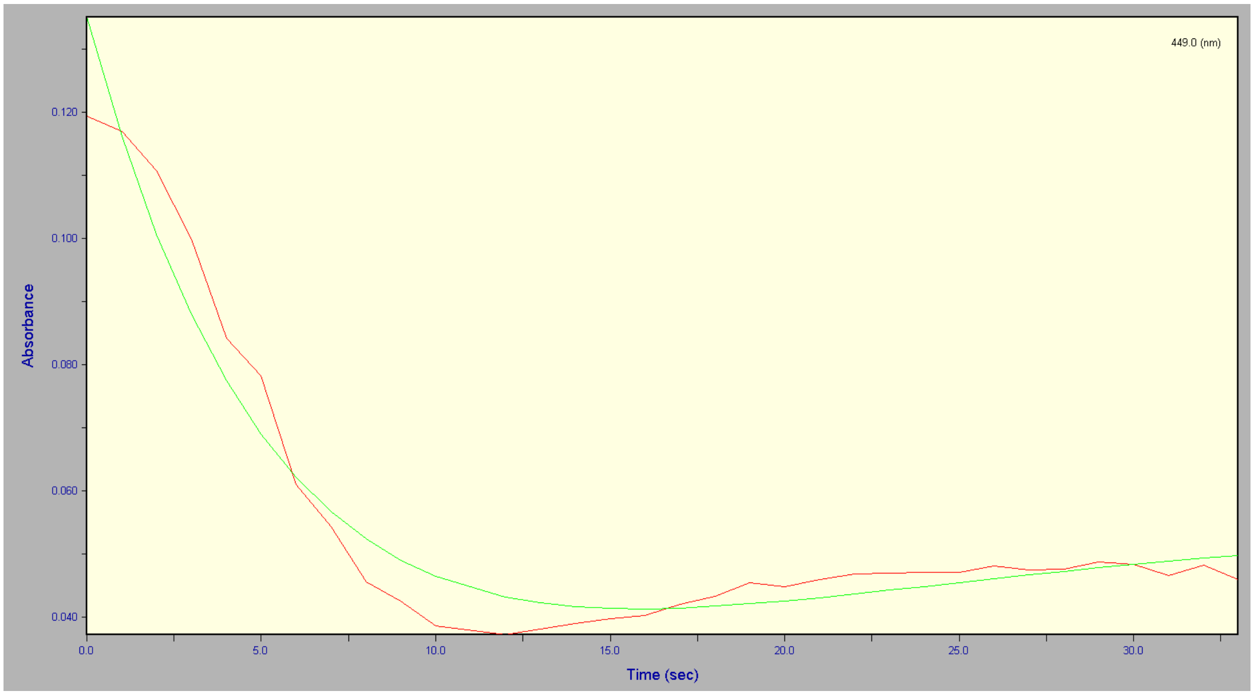

Figure S49. SPECFIT fitting of the titration of 145 µM **1** with 9.75 mM sodium periodate (green) vs. the observed absorbance at 449 nm (red).

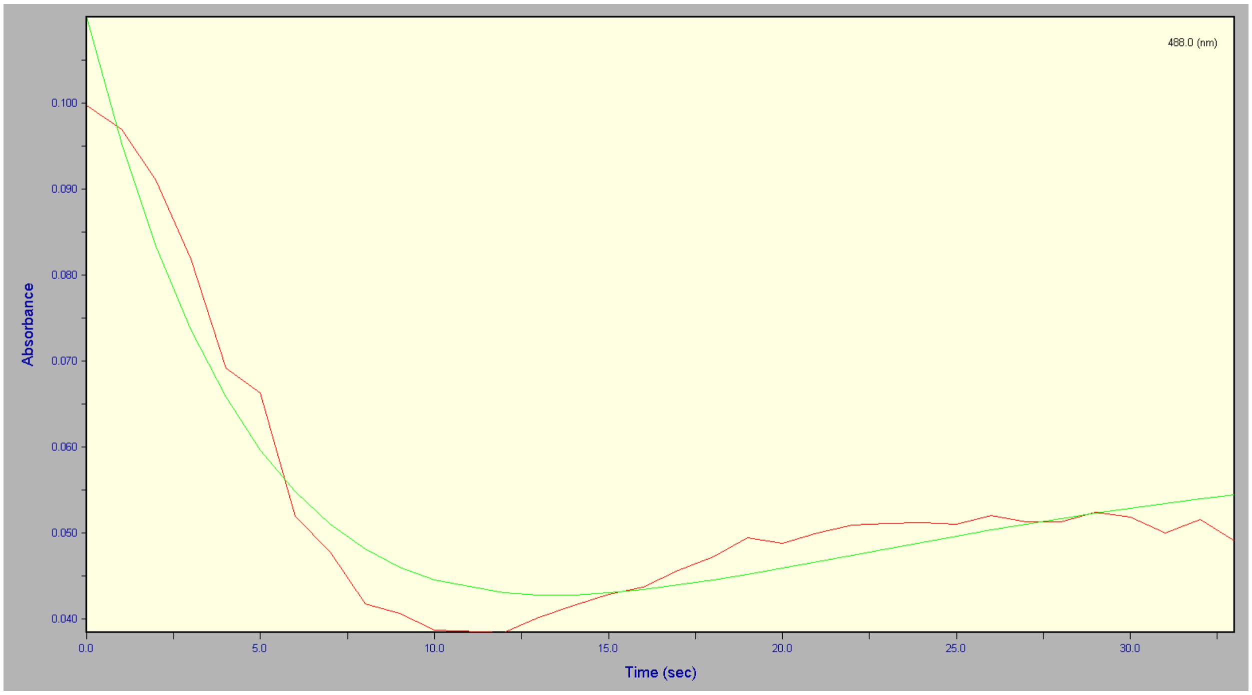

Figure S50. SPECFIT fitting of the titration of 145 µM **1** with 9.75 mM sodium periodate (green) vs. the observed absorbance at 488 nm (red).

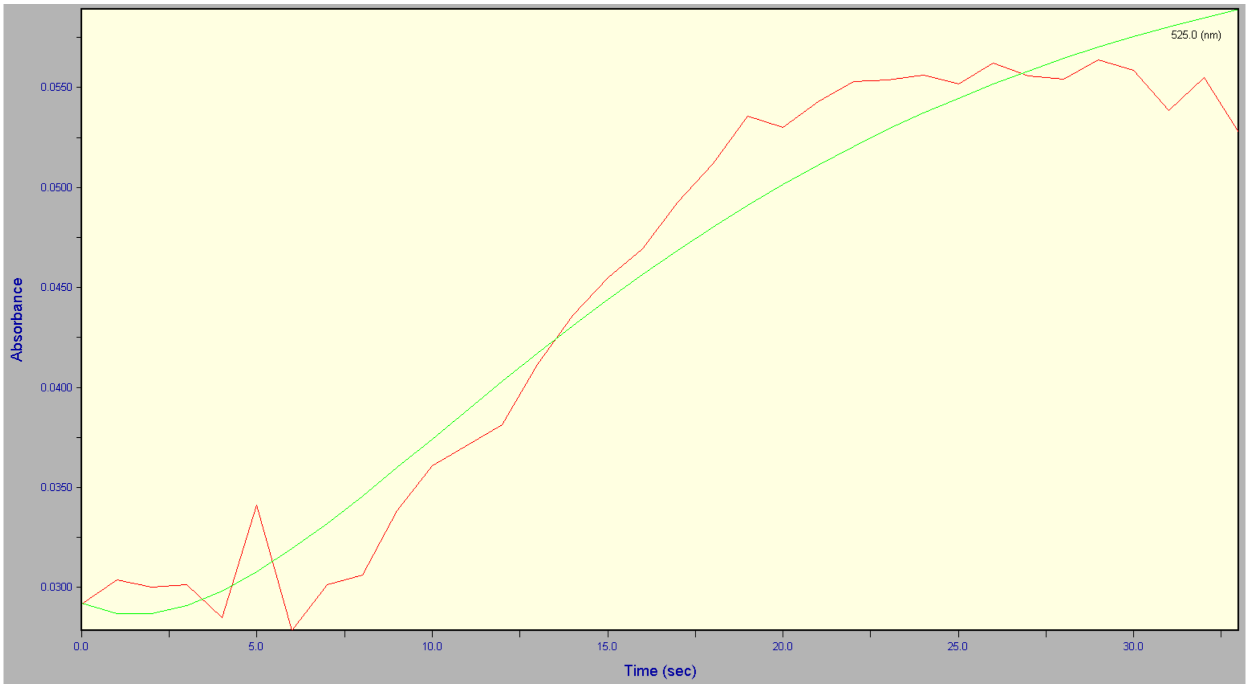

Figure S51. SPECFIT fitting of the titration of 145 µM **1** with 9.75 mM sodium periodate (green) vs. the observed absorbance at 525 nm (red).

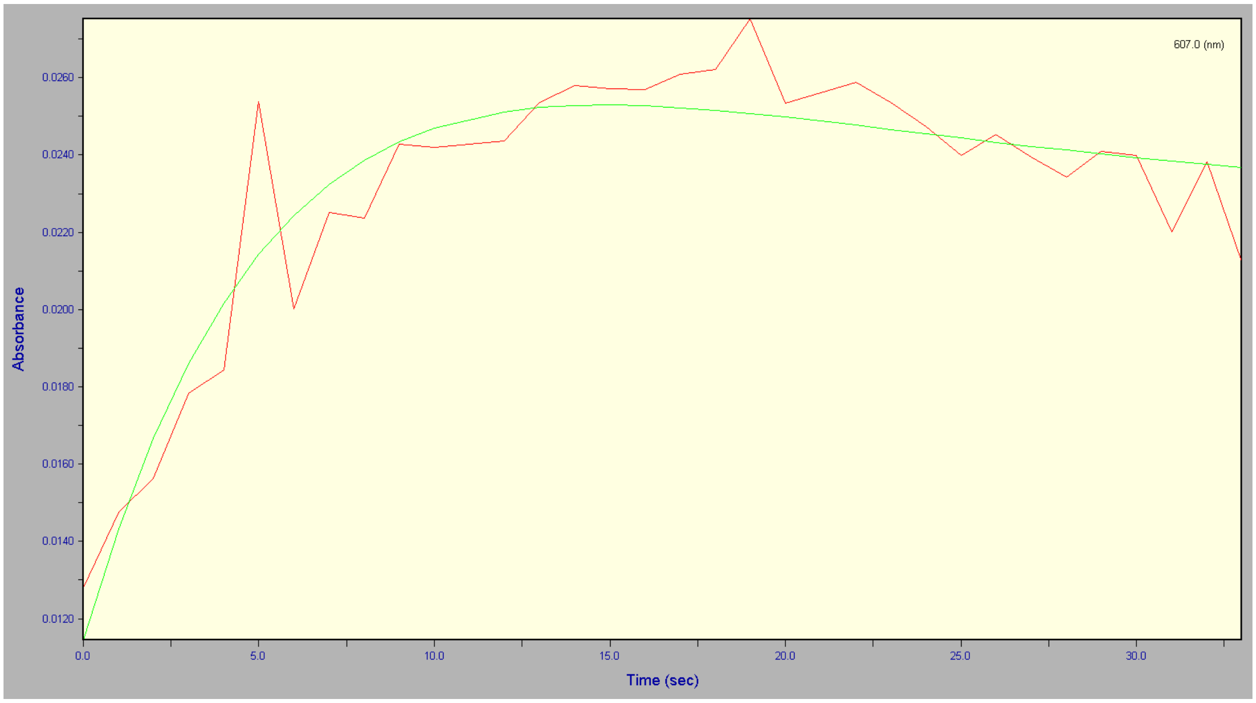

Figure S52. SPECFIT fitting of the titration of 145 µM **1** with 9.75 mM sodium periodate (green) vs. the observed absorbance at 607 nm (red).

Figure S53. SPECFIT fitting of the titration of 145 µM **1** with 9.75 mM sodium periodate (green) vs. the observed absorbance at 652 nm (red).

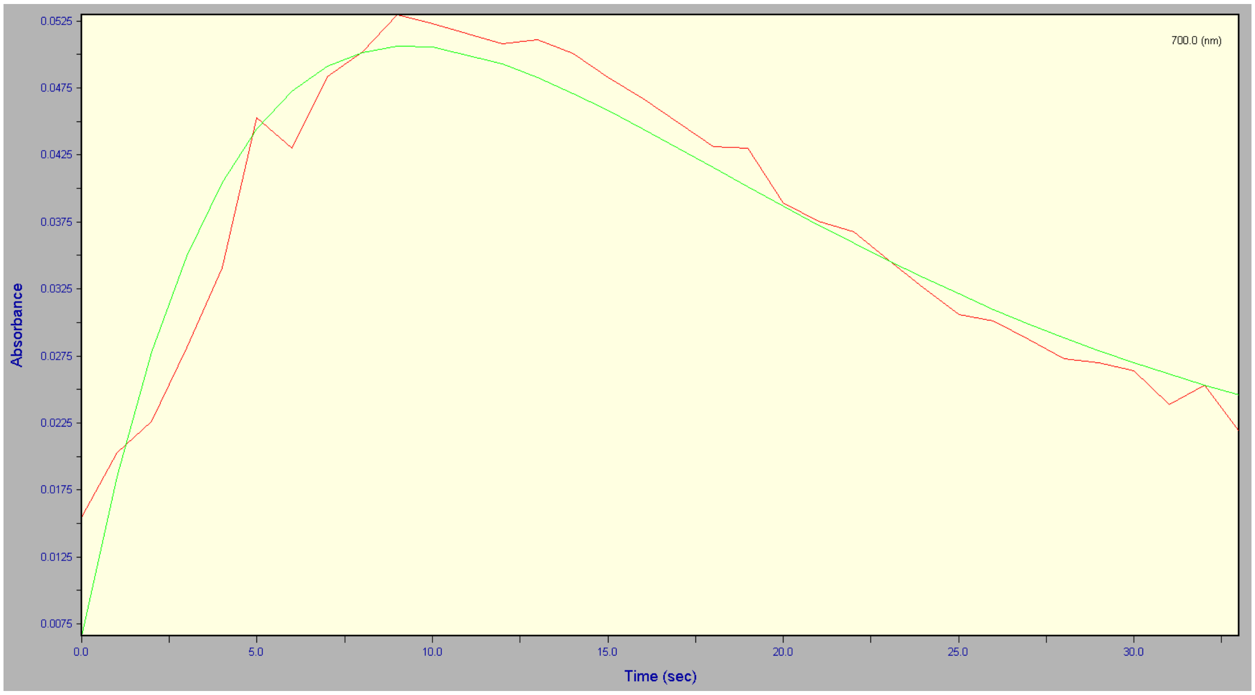

Figure 54. SPECFIT fitting of the titration of 145 μM **1** with 9.75 mM sodium periodate (green) vs. the observed absorbance at 700 nm (red).

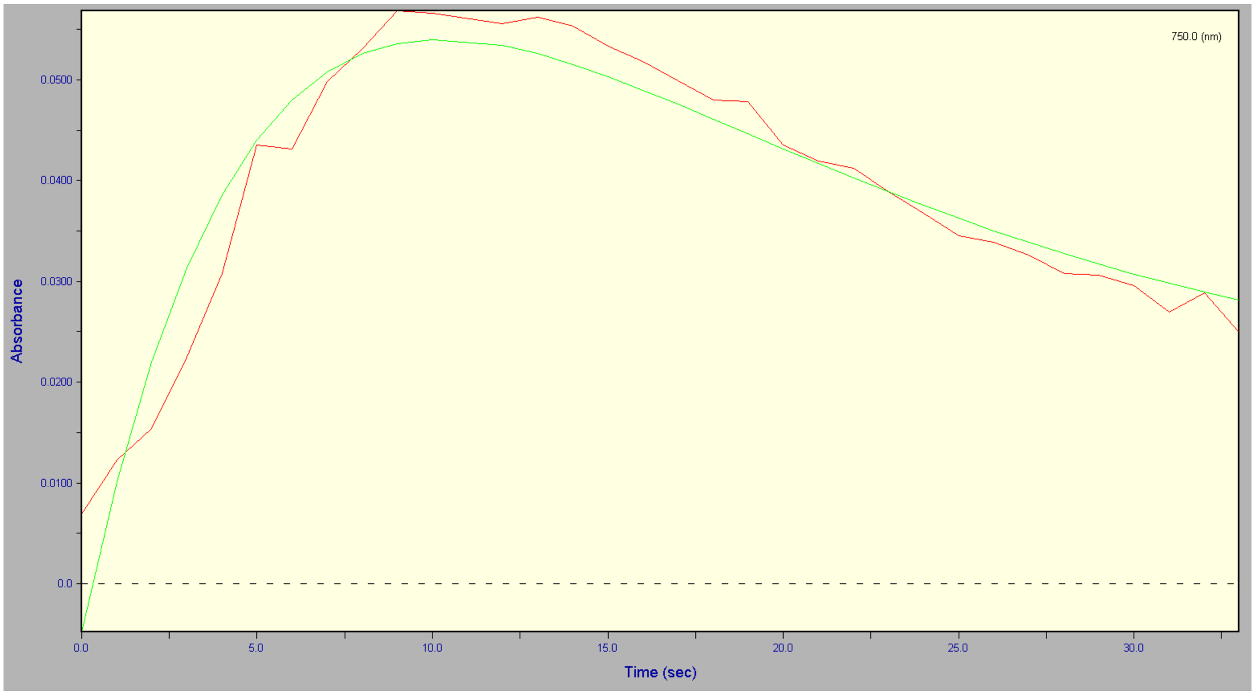

Figure 55. SPECFIT fitting of the titration of 145 μM **1** with 9.75 mM sodium periodate (green) vs. the observed absorbance at 750 nm (red).

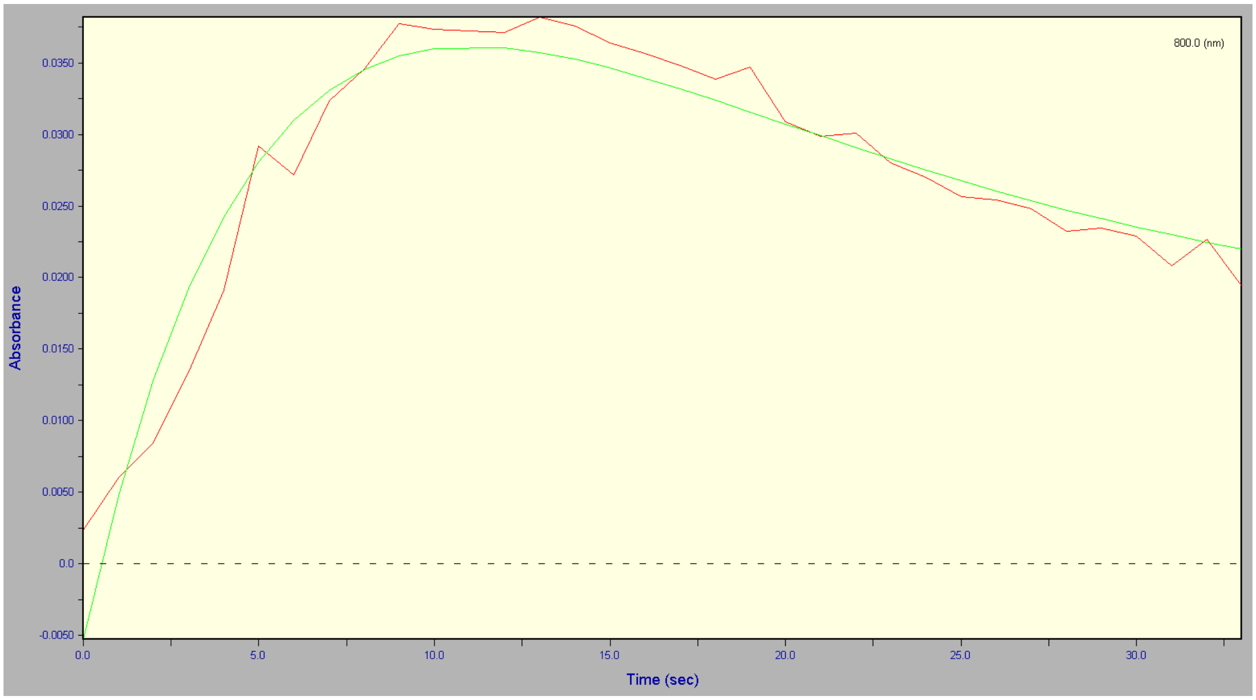

Figure 56. SPECFIT fitting of the titration of 145 μM **1** with 9.75 mM sodium periodate (green) vs. the observed absorbance at 800 nm (red).

Table S1. Crystallographic Data

	1	2
formula	C37 H42 Fe2 N8 O14 S3	C36 H63 Fe2 N6 O17.5 S2
fw	1030.67	1035.73
color, habit	Dark Green, Blocks	Dark Red, Prisms
crystal size, mm	0.13x0.1x0.08	0.3x0.2x0.12
crystal system	Monoclinic	Orthorhombic
space group	P 21/n	P b c n
a, A	12.8773(10)	16.051(5)
b, A	24.3493(19)	19.314(6)
c, A	13.5153(10)	14.958(4)
a, deg	90.00	90.00
b, deg	102.513(1)	90.00
g, deg	90.00	90.00
V, A3	4137.1(5)	4637(2)
Z	4	4
F(000)	2128	2116
dcalc, g/cm3	1.655	1.483
m(Mo Ka), mm-1	0.932	0.787
trans coeff	0.889 - 0.928	0.574 - 0.746
T, K	100(2)	100(2)
radiation, A	0.71073	0.71073
theta range, deg	$2.15 < \theta < 27.10$	$2.11 < \theta < 26.72$
reflns measd	46117	39053
uniq reflns	9116	4910
R(int)	0.0262	0.0464
data/restraints/params	9116/0/734	4910/0/311
R1	0.0278	0.0878
wR2	0.0708	0.2044
GOF	1.040	1.171
max/mean shift/esd	0.002/0.000	0.000/0.000
max/min diff. peaks	0.614/-0.351	1.243/-0.726

Table S2. Interatomic Distances (Å) and Angles (º) for **1**

Fe1-O1	1.7914(12)	Fe1-O3	2.0219(12)
Fe1-N3	2.1337(15)	Fe1-N1	2.1356(15)
Fe1-N4	2.1364(14)	Fe1-N2	2.2354(15)
Fe2-O1	1.8061(12)	Fe2-O2	1.9645(12)
Fe2-N7	2.1214(14)	Fe2-N5	2.1343(15)
Fe2-N6	2.2159(14)	Fe2-N8	2.2205(15)
S1-O5	1.4395(14)	S1-O4	1.4543(13)
S1-O3	1.5015(12)	S1-O2	1.5159(13)
S2-O8	1.4425(14)	S2-O6	1.4451(14)
S2-O9	1.4580(14)	S2-O7	1.5813(14)
S3-O13	1.4397(14)	S3-O11	1.4481(14)
S3-O10	1.4491(14)	S3-O12	1.5869(14)
O1M-C1M	1.429(3)	N1-C1	1.345(2)
N1-C5	1.346(2)	N2-C13	1.481(2)
N2-C7	1.485(2)	N2-C6	1.488(2)
N3-C8	1.346(2)	N3-C12	1.349(2)
N4-C18	1.349(2)	N4-C14	1.352(2)
N5-C19	1.346(2)	N5-C23	1.347(2)
N6-C31	1.482(2)	N6-C24	1.485(2)
N6-C25	1.491(2)	N7-C36	1.343(2)
N7-C32	1.345(2)	N8-C26	1.342(2)
N8-C30	1.347(2)	C1-C2	1.383(3)
C2-C3	1.389(3)	C3-C4	1.388(3)
C4-C5	1.393(3)	C5-C6	1.505(3)
C7-C8	1.509(3)	C8-C9	1.390(3)
C9-C10	1.382(3)	C10-C11	1.392(3)
C11-C12	1.379(3)	C13-C14	1.502(2)
C14-C15	1.387(2)	C15-C16	1.390(3)
C16-C17	1.387(3)	C17-C18	1.383(2)
C19-C20	1.381(3)	C20-C21	1.386(3)
C21-C22	1.387(3)	C22-C23	1.386(2)
C23-C24	1.512(2)	C25-C26	1.508(2)
C26-C27	1.388(3)	C27-C28	1.384(3)
C28-C29	1.387(3)	C29-C30	1.382(3)
C31-C32	1.506(2)	C32-C33	1.383(2)
C33-C34	1.384(3)	C34-C35	1.382(3)
C35-C36	1.377(3)		
O1-Fe1-O3	99.13(5)	O1-Fe1-N3	97.71(6)
O3-Fe1-N3	162.66(5)	O1-Fe1-N1	104.79(6)
O3-Fe1-N1	87.86(5)	N3-Fe1-N1	83.90(6)
O1-Fe1-N4	102.25(6)	O3-Fe1-N4	86.05(5)
N3-Fe1-N4	94.38(5)	N1-Fe1-N4	152.89(6)
O1-Fe1-N2	176.14(6)	O3-Fe1-N2	84.49(5)

N3-Fe1-N2	78.78(6)	N1-Fe1-N2	76.59(5)
N4-Fe1-N2	76.55(5)	O1-Fe2-O2	100.36(5)
O1-Fe2-N7	94.24(5)	O2-Fe2-N7	106.46(6)
O1-Fe2-N5	96.15(5)	O2-Fe2-N5	97.33(6)
N7-Fe2-N5	151.83(6)	O1-Fe2-N6	98.50(5)
O2-Fe2-N6	160.41(5)	N7-Fe2-N6	77.25(5)
N5-Fe2-N6	75.35(5)	O1-Fe2-N8	174.44(5)
O2-Fe2-N8	84.08(5)	N7-Fe2-N8	81.22(5)
N5-Fe2-N8	86.53(6)	N6-Fe2-N8	77.42(5)
O5-S1-O4	114.23(8)	O5-S1-O3	110.88(8)
O4-S1-O3	107.73(7)	O5-S1-O2	109.09(8)
O4-S1-O2	107.67(8)	O3-S1-O2	106.95(7)
O8-S2-O6	114.72(8)	O8-S2-O9	111.95(9)
O6-S2-O9	113.25(9)	O8-S2-O7	104.88(8)
O6-S2-O7	106.55(8)	O9-S2-O7	104.40(8)
O13-S3-O11	113.93(9)	O13-S3-O10	113.93(9)
O11-S3-O10	112.29(9)	O13-S3-O12	103.37(9)
O11-S3-O12	106.31(9)	O10-S3-O12	105.94(9)
Fe1-O1-Fe2	134.34(7)	S1-O2-Fe2	132.35(8)
S1-O3-Fe1	128.12(7)	C1-N1-C5	119.18(15)
C1-N1-Fe1	124.38(12)	C5-N1-Fe1	115.65(12)
C13-N2-C7	109.60(14)	C13-N2-C6	110.47(14)
C7-N2-C6	112.58(15)	C13-N2-Fe1	107.24(10)
C7-N2-Fe1	110.16(11)	C6-N2-Fe1	106.62(10)
C8-N3-C12	118.84(16)	C8-N3-Fe1	117.34(12)
C12-N3-Fe1	123.15(12)	C18-N4-C14	118.86(15)
C18-N4-Fe1	124.33(12)	C14-N4-Fe1	116.74(11)
C19-N5-C23	119.51(16)	C19-N5-Fe2	124.89(13)
C23-N5-Fe2	115.52(12)	C31-N6-C24	112.52(14)
C31-N6-C25	111.11(14)	C24-N6-C25	110.54(14)
C31-N6-Fe2	105.28(10)	C24-N6-Fe2	104.77(10)
C25-N6-Fe2	112.38(10)	C36-N7-C32	119.22(15)
C36-N7-Fe2	124.64(12)	C32-N7-Fe2	115.84(11)
C26-N8-C30	118.55(16)	C26-N8-Fe2	116.03(12)
C30-N8-Fe2	124.76(12)	N1-C1-C2	122.36(17)
C1-C2-C3	118.46(17)	C4-C3-C2	119.63(17)
C3-C4-C5	118.58(17)	N1-C5-C4	121.71(16)
N1-C5-C6	116.99(16)	C4-C5-C6	121.16(16)
N2-C6-C5	111.73(15)	N2-C7-C8	114.80(15)
N3-C8-C9	121.70(17)	N3-C8-C7	117.44(16)
C9-C8-C7	120.81(16)	C10-C9-C8	119.31(18)
C9-C10-C11	118.81(18)	C12-C11-C10	119.01(18)
N3-C12-C11	122.23(17)	N2-C13-C14	110.94(14)
N4-C14-C15	121.54(16)	N4-C14-C13	116.04(15)
C15-C14-C13	122.28(16)	C14-C15-C16	119.25(16)
C17-C16-C15	119.09(17)	C18-C17-C16	118.78(17)

N4-C18-C17	122.35(16)	N5-C19-C20	121.80(18)
C19-C20-C21	118.97(19)	C20-C21-C22	119.27(18)
C23-C22-C21	118.98(18)	N5-C23-C22	121.46(17)
N5-C23-C24	115.29(15)	C22-C23-C24	123.22(17)
N6-C24-C23	107.89(14)	N6-C25-C26	114.13(14)
N8-C26-C27	121.99(17)	N8-C26-C25	117.73(15)
C27-C26-C25	120.24(16)	C28-C27-C26	119.01(18)
C27-C28-C29	119.31(18)	C30-C29-C28	118.37(18)
N8-C30-C29	122.77(17)	N6-C31-C32	109.20(14)
N7-C32-C33	121.81(16)	N7-C32-C31	115.03(15)
C33-C32-C31	123.13(16)	C32-C33-C34	118.61(16)
C35-C34-C33	119.44(16)	C36-C35-C34	119.01(17)
N7-C36-C35	121.83(16)		

Table S3. Interatomic Distances (Å) and Angles (°) for **2**

Fe1-O1	1.7880(17)	Fe1-O2	2.040(3)
Fe1-O3	1.970(4)	Fe1-N3	2.174(4)
Fe1-N2	2.140(4)	Fe1-N1	2.226(4)
S1-O3	1.501(4)	S1-O4	1.455(4)
S1-O5	1.433(5)	S1-O6	1.457(5)
O2-C2	1.458(6)	O1-Fe1a	1.7880(17)
O8-C17	1.366(10)	O9-C18B	1.366(10)
O9-C18A	1.46(2)	C19-O20	1.01(3)
O19-C20	1.01(3)	N1-C1	1.477(6)
N1-C11	1.480(6)	N1-C5	1.490(6)
N2-C16	1.331(7)	N2-C12	1.358(6)
N3-C10	1.337(6)	N3-C6	1.341(6)
C1-C2	1.529(7)	C2-C3	1.522(7)
C2-C4	1.527(7)	C5-C6	1.501(7)
C6-C7	1.400(7)	C7-C8	1.363(8)
C8-C9	1.390(9)	C9-C10	1.371(8)
C11-C12	1.501(7)	C12-C13	1.375(7)
C13-C14	1.390(8)	C14-C15	1.378(8)
C15-C16	1.385(8)		
O1-Fe1-O2	100.91(16)	O1-Fe1-O3	104.79(12)
O2-Fe1-O3	93.16(15)	O1-Fe1-N1	168.02(12)
O1-Fe1-N2	103.45(17)	O1-Fe1-N3	91.34(13)
O2-Fe1-N1	78.24(14)	O2-Fe1-N2	155.10(14)
O2-Fe1-N3	87.89(14)	O3-Fe1-N1	87.19(15)
O3-Fe1-N2	85.60(15)	O3-Fe1-N3	163.30(15)
N1-Fe1-N2	76.86(15)	N1-Fe1-N3	76.69(15)
N2-Fe1-N3	86.47(15)	O3-S1-O4	107.5(2)
O3-S1-O5	108.8(3)	O3-S1-O6	107.9(3)
O4-S1-O5	113.9(3)	O4-S1-O6	108.7(3)
O5-S1-O6	109.9(3)	S1-O3-Fe1	150.7(2)
C2-O2-Fe1	120.1(3)	Fe1-O1-Fe1a	142.1(3)
C1-N1-C11	112.2(4)	C1-N1-C5	113.4(4)
C5-N1-C11	109.5(4)	C1-N1-Fe1	103.7(3)
C11-N1-Fe1	104.3(3)	C5-N1-Fe1	113.4(3)
C12-N2-C16	118.9(4)	C16-N2-Fe1	125.9(3)
C12-N2-Fe1	115.1(3)	C6-N3-C10	118.3(4)
C10-N3-Fe1	123.4(4)	C6-N3-Fe1	118.3(3)
N1-C1-C2	113.1(4)	O2-C2-C3	109.0(4)
C3-C2-C4	109.6(4)	O2-C2-C1	106.3(4)
O2-C2-C4	108.2(4)	C1-C2-C3	115.2(4)
C1-C2-C4	108.3(4)	N1-C5-C6	113.4(4)
N3-C6-C7	121.2(5)	N3-C6-C5	117.9(4)
C5-C6-C7	121.0(5)	C6-C7-C8	119.6(5)

C7-C8-C9	119.1(5)	C8-C9-C10	118.2(5)
N3-C10-C9	123.6(5)	N1-C11-C13	109.9(4)
N2-C12-C13	121.6(5)	N2-C12-C11	115.0(4)
C11-C12-C13	123.3(4)	C12-C13-C14	118.7(5)
C13-C14-C15	119.7(5)	C14-C15-C16	118.2(5)
N2-C16-C15	122.6(5)		